



BIOENGINEERING UNIT

MSc. THESIS

**Characterising hand movements with
high-density surface electromyography**

Author:

Thomas HARRISON

Member, IEEE

Supervisor:

Dr. Heba LAKANY

Senior Member, IEEE

August 2011

Declaration of Authenticity and Author's Rights

This thesis is the result of the authors original research. It has been composed by the author and has not been previously submitted for examination which has led to the award of a degree.

The copyright of this thesis belongs to the author under the terms of the United Kingdom Copyright Acts as qualified by University of Strathclyde Regulation 3.50. Due acknowledgement must always be made of the use of any material contained in, or derived from, this thesis.

Signed: **Date:**/...../ 2011

Acknowledgements

I am grateful to many people for all the help and support I have received during this project. In particular I would like to thank my supervisor, Dr. Heba Lakany, who has been so patient with me, and Eve Bird who has been incredibly supportive and understanding during the period of writing up (and also helped me with the pre-testing).

I am also extremely grateful to all the individuals who kindly volunteered their (rather limited) time to participate in these experiments. These subjects are: Radhika, Sibani, Claire, Mayank, Monica and Mark (who selflessly shaved his arm for the experiment).

Abstract

High-density surface electromyography (HD sEMG) is a recent development in the field of neurorehabilitation allowing simultaneous recording of many, spatially differentiated motor unit action potentials (MUAPs). The available literature on studies using HD sEMG is reviewed as a preamble to the experiment. Only one of these is related to prosthetic control and this utilised only a very crude approximation of HD sEMG³¹. Information relating to muscle physiology, electromyography (EMG) and wavelet analysis is also discussed to facilitate understanding of the methods.

Using two 64-channel HD electrode-arrays, muscle activation during four different hand movements (and a negative control) were recorded from the extensor digitorum superficialis and flexor digitorum communis of five subjects.

Relative wavelet packet energy (RWPE) is the scale-dependent relative energy distribution of a signal at each frequency band after decomposition with the wavelet packet transform and has been previously applied to sEMG with some success²⁹. Wavelet packet analysis is carried out offline on the 128-channel recordings and the relative spectral energy density is calculated for each hand movement. Mean values and standard deviations are shown for visualization. Three-way ANOVA is computed for interaction effects between movement, location and firing frequency. Some significant interactions are found ($p \approx 0$), but many interactions are not significant suggesting modifications to the experimental design would have to be made for application to prosthetic control.

Contents

1	Introduction	1
1.1	Background and aim of the study	1
1.2	Organisation of the thesis	1
2	Surface electromyography	3
2.1	Introduction	3
2.2	Muscle physiology	3
2.2.1	The neuromuscular system	3
2.2.2	Muscle fibres	4
2.2.3	Motor units	4
2.2.4	Motor unit action potentials	5
2.2.5	Motor unit recruitment	6
2.2.6	Volume conduction effects	7
2.3	Electromyography	7
2.3.1	Intramuscular EMG	7
2.3.2	Surface EMG	8
2.3.3	Monopolar recording	8
2.3.4	Non-propagating components	8
2.4	Interference	8
2.4.1	Noise	9
2.4.2	Signal artefacts	9
2.4.3	Superimposition	9
2.4.4	The interference signal	9

2.5	Multichannel sEMG	10
2.5.1	Spatial filtering	10
2.5.2	The linear array	12
2.5.3	The two-dimensional montage	12
2.5.4	High-density arrays	12
2.5.5	Spatial sampling	12
2.6	Summary	13
3	High-Density Surface Electromyography: a review of the literature so far	14
3.1	Introduction	14
3.1.1	Span of the field	14
3.1.2	Review structure	15
3.1.3	Research groups	15
3.2	Challenges of HD sEMG	16
3.2.1	Advantages	16
3.2.2	The interference signal	16
3.2.3	Validation of results	17
3.3	Existing Reviews	17
3.4	HD array design	18
3.4.1	Number of channels	18
3.4.2	Spatial sampling	18
3.4.3	Spatial filtering	19
3.4.4	Spatial density	19
3.4.5	Array size	19
3.4.6	Attachment	20
3.4.7	Electrode size	20
3.5	Decomposition techniques	20

3.5.1	Difficulties	21
3.5.2	Spike-triggered averaging	21
3.5.3	Interactive techniques	21
3.5.4	Automatic techniques	23
3.5.5	Validation of results	24
3.6	Other experimental aims	25
3.6.1	Motor unit number estimation	25
3.6.2	Topographical information	25
3.6.3	Prosthetic control	26
3.6.4	Propagation	26
3.7	Conclusion	27
4	Signal analysis	31
4.1	Introduction	31
4.2	Fourier analysis	31
4.2.1	Fourier transforms	31
4.3	Wavelets	32
4.3.1	Basis functions	32
4.3.2	Dimensions	33
4.3.3	Energy	34
4.4	Wavelet transforms	35
4.4.1	The continuous wavelet transform	35
4.4.2	The discrete wavelet transform	35
4.4.3	The wavelet packet transform	36
4.5	summary	37
5	Design considerations	38
5.1	Introduction	38

5.2	Data acquisition	38
5.2.1	Wrist movement	38
5.2.2	Extrinsic hand musculature	39
5.2.3	Electrode placement	39
5.2.4	Array parameters	39
5.2.5	Recording parameters	40
5.3	Signal processing	40
5.3.1	Muscle characterization	41
5.3.2	Wavelet analysis	41
5.3.3	Wavelet transform	41
5.4	Statistical analysis	42
5.4.1	Variables	42
5.4.2	Method	42
5.5	Summary	43
6	Methods	44
6.1	HD sEMG Acquisition	44
6.1.1	Subjects	44
6.1.2	Equipment	44
6.1.3	Setup	45
6.1.4	Protocol	46
6.2	Data analysis	47
6.2.1	Signal conversion	47
6.2.2	Wavelet Packet analysis	47
6.2.3	Statistical analysis	48
7	Results	49
7.1	Graphs	50

7.2	Common features	57
7.3	Discriminant features	58
7.3.1	Subject 1	58
7.3.2	Subject 2	58
7.3.3	Subject 3	58
7.3.4	Subject 4	59
7.3.5	Subject 5	59
8	Discussion	60
8.1	Principle findings	60
8.2	Alternative research	62
8.3	Limitations	62
8.4	Future work	63
8.5	Conclusion	63
9	Summary and Conclusion	64
9.1	Introduction	64
9.2	Summary of chapters	64
9.3	Evaluation	65
	Appendices	67
	Bibliography	91

List of Tables

3.1	A timeline of the literature. Shaded rows denote literature reviews.	28
3.2	The experimental parameters used within this review, part 1	29
3.3	The experimental parameters used within this review, part 2	30
7.1	Results of a 3-way ANOVA between selected conditions	57
1	Results of 3-way ANOVA for Subject 1 for interactions between hand and pinch flexion.	70
2	Results of 3-way ANOVA for Subject 2 for interactions between hand and pinch flexion.	70
3	Results of 3-way ANOVA for Subject 3 for interactions between hand and pinch flexion.	70
4	Results of 3-way ANOVA for Subject 3 for interactions between hand and pinch extension.	71
5	Results of 3-way ANOVA for Subject 4 for interactions between hand and pinch flexion.	71
6	Results of 3-way ANOVA for Subject 4 for interactions between hand and pinch extension.	71
7	Results of 3-way ANOVA for Subject 5 for interactions between hand and pinch flexion.	72

List of Figures

2.1	A representation of the muscle physiology at decreasing scales. Picture from MedicalNanoTec.com, ©2011.	4
2.2	The triphasic shape of the MUAP is brought about through a sudden depolarization stage followed by a more gradual repolarization stage.	5
2.3	MUAPs have a much smaller duration than the muscle fibre twitch response. A succession of MUAPs, with a rate of about 35 Hz or above will results in a temporal summation of contraction, leading to a higher force. Picture from Datta et al. ⁸ ©2007, The Open University.	6
2.4	Spatial filters are the weighted sums of various spatial arrangements of electrodes, causing high-pass filtering in the spatial domain. Adapted from Farina et al. ¹⁵ , ©2008, The American Physiological Society.	10
2.5	A MUAP recorded with monopolar or bipolar montage. The dotted lines represent the location of far-field phenomena, note these are suppressed in the bipolar derivation and the waveform is altered. Figure from Zwarts et al ⁶² ., ©2003, Wiley Periodicals.	11
2.6	A longitudinal array of surface electrodes with several spatial filters applied. The top two are double differential with different electrode inputs (note the inter-electrode distances remain the same). Details are enhanced with higher derivatives making MUAPs more easily identifiable. Figure from Reucher et al. ⁴⁷ , ©1987, IEEE.	11
2.7	An example of an early high-density sEMG array as developed by Blok et al. ² ©2002, American Institute of Physics.	13
4.1	Four different wavelet: (A) the db2 and (B) db5 wavelets, invented by Ingrid Daubechie, and two biorthogonal wavelets, (c) bior1.3 and (d) bior1.5. Image taken from www.SpringerImages.com ©2011	33
4.2	Representation of a sawtooth signal with 16 scaled and time-shifted versions of the db4 wavelet. Image taken from Bruce et al., ⁴ ©1996, IEEE	34

4.3	The signal is decomposed through iterations of the scaling wavelet and the analysing wavelet. New details are assumed to contain redundancy due to the preservation of the details from the initial decomposition. Picture from www.originlab.com , ©2011	36
4.4	A visual representation of the wavelet packet decomposition process. The raw signal, S, is successively divided into high (details, D) and low (approximations,A) scales, doubling the number of scale bands with each iteration. Picture from www.mathworks.com , ©2011	37
5.1	Mid-wrist musculature (cross-section). Picture taken from Wikipedia.org , ©2011.	40
6.1	The layout of the 64-channel HD array used for sEMG recording. The black channels indicate the split between output ports. Note that columns run antiparallel to each other. Array (ELSCH064R3S) and diagram supplied by OT Bioelettronica, Torino, Italy, ©2011	45
6.2	Two foam covered blocks were used as armrests. The base of each was made from wood and two metal rods maintained a fixed difference. The rods had various holes in the ends so that the separation of the blocks could be adjusted for physiological variation in arm length.	46
6.3	A thermosetting acrylic sheet was cut and moulded around a hollow cylinder. A slit allowed the finger tips to slide underneath a section, thus isometric extension and flexion of the fingers was possible. A cord looped through the cylinder and provided isometric resistance against thumb extension. During the experiment the device was mounted to a rod in the desk (not shown).	46
7.1	Mean values and standard deviations for the (negative) control condition for Subject 1. Controls were taken between each movement set, thus are representative of the entire experimental duration	50
7.2	Mean values and standard deviations for the (negative) control condition for Subject 2. Controls were taken between each movement set, thus are representative of the entire experimental duration	50
7.3	Mean values and standard deviations for the (negative) control condition for Subject 3. Controls were taken between each movement set, thus are representative of the entire experimental duration	51

7.4	Mean values and standard deviations for the (negative) control condition shown for Subject 4. Controls were taken between each movement set, thus are representative of the entire experimental duration	51
7.5	Mean values and standard deviations for the (negative) control condition shown for Subject 5. Controls were taken between each movement set, thus are representative of the entire experimental duration	51
7.6	The RWPE coefficients for subject 1. Mean values and standard deviations for the (negative) control condition shown. Controls were taken between each movement set, thus are representative of the entire experimental duration. . . .	52
7.7	The RWPE coefficients for subject 2. Mean values and standard deviations for the (negative) control condition shown. Controls were taken between each movement set, thus are representative of the entire experimental duration. . . .	53
7.8	The RWPE coefficients for subject 3. Mean values and standard deviations for the (negative) control condition shown. Controls were taken between each movement set, thus are representative of the entire experimental duration. . . .	54
7.9	The RWPE coefficients for subject 4. Mean values and standard deviations for the (negative) control condition shown. Controls were taken between each movement set, thus are representative of the entire experimental duration. . . .	55
7.10	The RWPE coefficients for subject 5. Mean values and standard deviations for the (negative) control condition shown. Controls were taken between each movement set, thus are representative of the entire experimental duration. . . .	56

Chapter 1

Introduction

1.1 Background and aim of the study

High-density electromyography is a relatively new technology in the field of the biosignal analysis. A 2-dimensional array of electrodes is employed to locate the spatial distribution of bioelectrical sources. This complements the temporal analysis used by more conventional electromyographical recording methods, allowing extra dimensionality to the data.

The aim of this research project is to characterise hand movements using the extrinsic musculature of the wrist. It is hoped that this could lead to useful information for the design of a myoelectrically controlled prosthetic arm.

Wavelet packet analysis allows the rapid decomposition of data into equally spaced frequency bases. It is hoped that the merging of these two state-of-the-art techniques will allow neural drive to be characterised in a novel way.

The merging of wavelet analysis and high-density electromyography has only been carried out in a single study to date¹⁹ and this was for a very different purpose. In fact, the application of high-density electromyography to the field of neuroprosthetic is a rare occurrence in itself. These studies will be discussed in the following chapters.

1.2 Organisation of the thesis

This project has been divided up into chapters, the contents of which will be quickly summarised:

Chapter 2 is concerned with surface electromyography. This information is necessary for an

understanding of the concepts employed in the research, both of my own project and of the literature discussed. It culminates with a brief mention of the parameters associated with high-density electromyography, the subject of chapter 3.

Chapter 3 is a literature review of the papers concerned with high-density electromyography. The research aims within these studies is quite different to my own, yet the concepts used are still very relevant as they can be generalised to any signal acquisition with high-density arrays.

Chapter 4 explores some of the major themes in wavelet analysis and a comparison to Fourier analysis, a similar signal processing technique, is made.

In Chapter 5 the parameters that have been considered when designing the experiment are discussed. These are based upon the concepts explored in chapters 2, 3 and 4.

Chapter 6 explains the methods employed in the study itself, including acquisition of HD sEMG data, signal processing to obtain time-domain information and statistical analysis to ascertain the validity of the results.

Chapter 7 presents the results of the experiment. These results are discussed in Chapter 8. Some suggestions are made as to the limitations of the experimental design limitations and ways of overcoming these are posited.

Finally chapter 9 summarises and concludes the report. There are several appendices containing (respectively) a glossary of terms and acronyms, more detailed results and the MATLAB scripts written for the data analysis.

Chapter 2

Surface electromyography

2.1 Introduction

Electromyography is defined by the Concise Oxford English Dictionary (2001) as 'the recording of the electrical activity of muscle tissues by means of electrode'. Although its existence has been known for centuries, electromyography (EMG) has only gained widespread clinical use since the 1960s⁵². Primarily it is used to characterise motor functioning, yet the ability to extract signals of muscle intention from the surface makes it a useful tool for control of prosthetic limbs⁹. My project uses a recent adaptation of EMG which utilises many, evenly spaced electrodes attached to the skin to gain a substantial amount of information about the electromyographic signals beneath. An explanation of how this is achieved is discussed in this chapter. However, to understand this we must first look at how such signals are created and how they can be recorded.

2.2 Muscle physiology

2.2.1 The neuromuscular system

The signal properties of EMG are determined by the physiology of the neuromuscular system. Thus a brief discussion of this is necessary to understand how signals are created. For a more detailed discussion of the topic please refer to Vander's *Human Physiology*⁵⁵.

The evolution of a nervous system allowed animals to move in response to environmental stimuli. Hence one of the primary functions of the central nervous system (CNS) is motor output⁷. Motor neurons, or motoneurons, have their bodies in the spinal cord and through individual

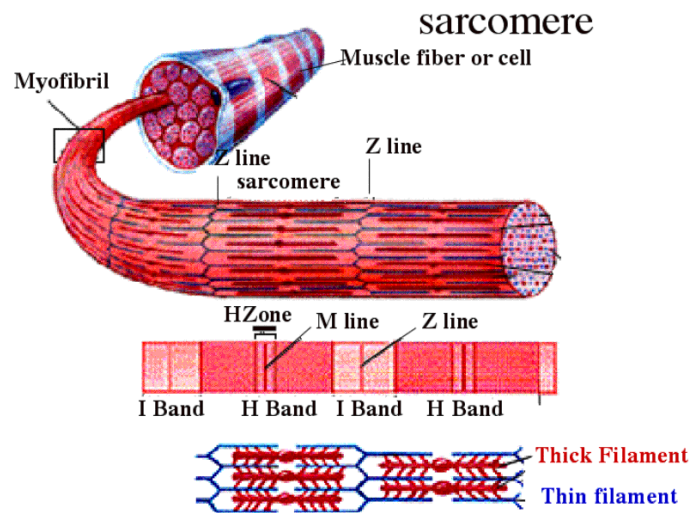


Figure 2.1 – A representation of the muscle physiology at decreasing scales. Picture from MedicalNanoTec.com, ©2011.

axonal projections convey information from the central nervous system to skeletal muscles⁷. They constitute about 60% of the neuronal projections to skeletal muscle¹⁶.

2.2.2 Muscle fibres

Skeletal muscle is composed of individual cells or muscle fibres. The muscle fibres are responsible for motile force and are innervated by α -motoneurons which connect via specialised synapses called neuromuscular junctions. The branched endings of these are called motor end plates and transmit the signal across a physical gap, to the muscle fibre, by release of a simple molecule called acetyl choline⁵. The membrane of the muscle fibre has a delicately controlled (resting) potential difference across it of about 70 mV⁶², i.e. it is maintained in an electrically polarized state. Within the muscle fibre are bundles of myofibril, containing two interlacing biopolymers: actin and myosin, which give it contractile properties¹⁶. Figure 2.1 gives a representation of the different scales within the muscle fibre.

2.2.3 Motor units

Many muscle fibres are innervated by a single α -motoneuron. The set of muscle fibres, along with their stimulatory motoneuron, are referred to as a motor unit². Thus the motor unit (MU) is the functional unit of the neuromuscular system¹⁹.

In primates, the size of motor units (MUs), i.e. the number of muscle fibres they contain, varies considerably⁵. Small muscles used for low-force, fine-control movement, such as in the hand have MUs with about 10-100 fibres. Whereas larger muscles which produce more force, such as

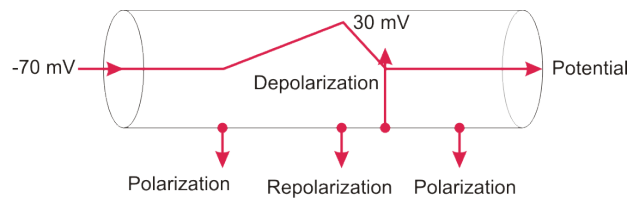


Figure 2.2 – The triphasic shape of the MUAP is brought about through a sudden depolarization stage followed by a more gradual repolarization stage.

the biceps, may have MUs with about 100-1000 fibres⁸. Due to their separate innervation, it is usually assumed that MUs have weak or none existent interaction with each other²⁶. However there is evidence to suggest that interneurons within the spinal cord allow motoneurons to inhibit one another⁵¹.

2.2.4 Motor unit action potentials

In a similar fashion to propagation of action potentials along an axon, signals are transmitted along the muscle fibre through electrochemical potential changes mediated by voltage-gated ion channels. A change in muscle fibre membrane potential (over a certain threshold) triggers the transient opening of nearby ion channels⁸. As a result adjacent sections are depolarized, thus the voltage change (i.e. the signal) is effectively propagated as a triphasic wave, as shown in figure 2.2. Due to the active nature of this process (i.e. energy is used) the signal characteristics are conserved. Thus, where v is the propagation velocity, the signal, s , can be represented by the following function of time, t , and space, z ⁶²:

$$s(z) = s(vt) \quad (2.1)$$

The propagating signal is called a motor unit action potential, or MUAP. A refractory period, which prevents ion-channels from reopening within a certain time period, ensures unidirectional propagation.

Calcium ions, released from a specialised compartment within the muscle fibre called the sarcolemma during the MUAP cause the muscle fibre to contract, or twitch⁵. This twitch will be simultaneous with that of other muscle fibres within the MU, producing a gross response.

As neural stimulation (neural drive) increases, the firing rates of active motoneurons are increased, thus more acetyl choline is released from the motor end plates. When the increase in MUAP firing rate increases sufficiently muscle fibre twitches can combine, producing a larger contraction⁸, as shown in figure 2.3. Thus, by temporal recruitment, a larger force is generated⁵²

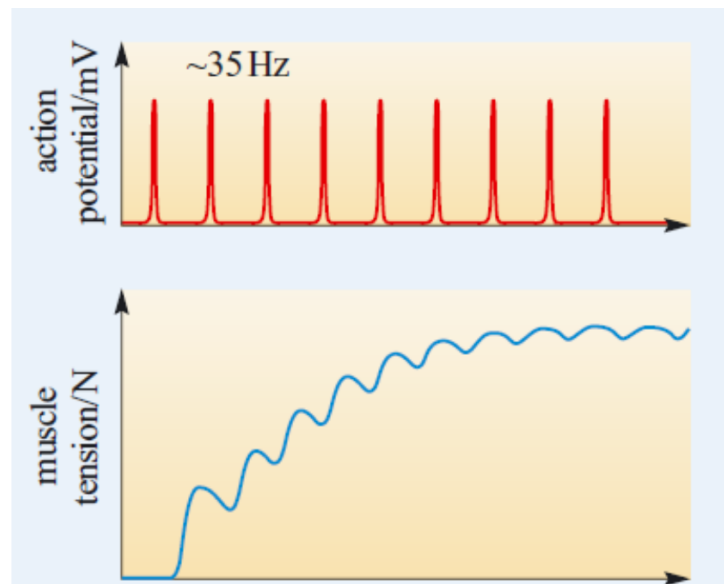


Figure 2.3 – MUAPs have a much smaller duration than the muscle fibre twitch response. A succession of MUAPs, with a rate of about 35 Hz or above will results in a temporal summation of contraction, leading to a higher force. Picture from Datta et al.⁸ ©2007, The Open University.

The refractory period means only a single MUAP can occur along a specific muscle fibre within a certain time period. Thus the size of the MUAP is not affected by neural drive. The shape of the MUAP is constant for each muscle fibre; the consequences of this on the EMG signal will be explored later.

2.2.5 Motor unit recruitment

As well as increased temporal recruitment, neural drive is mirrored by spatial recruitment of more active motor units⁵². Motor units are believed to be recruited in a specific order, relating to their thresholds of excitation⁵⁷. Smaller MUs with slower firing rates tend to be recruited (and derecruited) first, whereas the larger, faster firing (and therefore easier fatigued) MUs are reserved for higher forces and require a greater neural drive²³.

To sustain a contraction, each MU twitches at a roughly constant rate, however each rate is set slightly different so that simultaneously active MUs tend to fire asynchronously. A break down in asynchronicity has drastic consequences on the movement, as is seen with Parkinsons disease⁸. It also has consequences for the identification of individual MUAPs²⁴ as will be discussed in the following chapter.

2.2.6 Volume conduction effects

The tissues of the body are capable of transmitting charge, to varying degree. This means that aspects of the voltage change caused during MUAP propagation are radiated through the tissues to the surface⁵⁰. The 3-dimensional version of Ohm's law, often referred to as the principle of volume conduction, relates the dissipation of current within a field around a point of injection. The voltage at any point, V_j , can be approximated with knowledge of the source current, I_i , distance from the source, r_{ij} , and the electrical conductivity of the medium between source and observation, σ , using the following function⁶²:

$$V_j = \frac{1}{4\pi\sigma} r_{ij} \quad (2.2)$$

This shows an inverse relationship between distance and surface energy. As the tissues surrounding MUs are inhomogeneous, they have different impedances to current flow, most noticeably subcutaneous fat. This results in a low-pass filtering effect, meaning the high-frequency detail of individual MUAPs is lost, making them appear more similar at the surface²⁶. There appears to be high variation as to the degree of MUAP feature attenuation between subjects²¹.

2.3 Electromyography

Now that the underlying physiology has been explained we are in a position to look at EMG itself. The different types of EMG will be examined and the advantages and limitations of each will be discussed.

2.3.1 Intramuscular EMG

Intramuscular (or indwelling) electromyography (iEMG) is the most favoured approach for the electrodiagnostic study of muscles⁵⁰. It involves the insertion of a small electrode directly into the muscle, either as a needle or wire. The close proximity to the MU gives a very clear signal with little waveform attenuation from volume conductor effects⁴¹. The small recording area of the electrode limits the number of MUs in the signal, thus their individual contributions can be distinguished by waveform³³.

The downside of iEMG is its invasive nature which causes discomfort with risk of injury and infection to subjects. These factors usually preclude its application on children, athletes and those in long-term therapy⁵⁸. It can also hinder the maintenance of steady MU discharge pattern³³. The disadvantage of their limited reception is that signals do not represent all muscle

fibres within the MU²⁴. Consequentially it is impossible to replicate the recording conditions in subsequent sessions and the reproducibility of results, along with the clinical tracking of pathologies, is compromised³³.

2.3.2 Surface EMG

An alternative to iEMG is the recording of MUAPs by placement of electrodes on the surface (sEMG). Due to a larger pickup area (consequence of electrode width and source distance) these will monitor the activity of a much larger number of MUs, i.e. its spatial selectivity is reduced⁴⁷. As discussed earlier, however, volume conduction effects lead to signal distortion. The effects of volume conduction on the sEMG have been extensively modelled through *in silico* simulation to try and quantify the tissue parameters affect the acquired signal (e.g. by Roeleveld et al.⁴⁸).

The sEMG has most of its spectral power below 400-500 Hz. To meet the Nyquist criterion for accurate sinewave detection a sampling rate of 1 kHz or above is required⁵².

2.3.3 Monopolar recording

A signal that is recorded independently with each electrode (or from a single electrode) is called a monopolar signal. It is a combination of all of the MUAPs within range and the contributions of each MU are difficult to separate⁶².

2.3.4 Non-propagating components

A monopolar-recorded MUAP will have the triphasic form shown in figure 2.2 which propagates from the motor endplate to the tendon. However two monophasic positive deflections also occur, one at the start and one at the end of the MUAP. These are non-propagating, with constant waveform. They are caused by generation effects at the motor end plate region and extinction effects at the muscle fibre-tendon boundary⁶². Due to their location in relation to the MUAP they are often referred to as far-field phenomena. Fortunately, they can be removed by use of a spatial filter, as will be discussed later.

2.4 Interference

The extraction of useful information from sEMG is hindered by several sources of interference: noise, signal artefacts and superimposition.

2.4.1 Noise

Noise is a certainty in any sEMG signal and has many causes, including: impedance between the electrode and the skin and amplifier noise. These sources are usually assumed to be white, Gaussian noise and can drown out low-amplitude signal components. An important factor in signal quality is the ratio of signal energy to noise, referred to as the signal-to-noise ratio (SNR).

2.4.2 Signal artefacts

Signals from other sources can also be recorded in the sEMG signal. These include other bioelectrical phenomena, such as the electrocardiogram, impedance spikes, due to relative movement between the electrode and the skin (electrode motion artefact), and electromagnetic components induced by nearby electrical equipment or wiring (powerline interference) producing a single frequency at around 50 Hz⁵².

2.4.3 Superimposition

From the definition of linear space³⁷:

Any two elements $x, y \in L$ uniquely determine a third element $x + y \in L$, called the sum of x and y , i.e. the addition of two vectors creates a third vector.

Similarly, two waveforms occupying the same temporal and spatial space will combine to form a new waveform. This is the principle of linear superposition⁵⁹. If these potentials are of similar polarity then their values are summed (constructive interference).

For every $x \in L$ there also exists an element $-x$, (its negative) such that $x + (-x) = 0$.

Thus wave-potentials of opposite polarity are subtracted from one another (destructive interference). In the context of EMG, superposition of potentials is referred to as superimposition, as the waves are effectively superimposed upon one another.

2.4.4 The interference signal

The sEMG signal is composed of many different motor unit contributions which are superimposed upon each other and, unfortunately, noise resulting in constructive and destructive interference. These processes therefore result in loss of information. Recordings from the surface are known as the interference signal. As the number of MUAPs is always greater than the number of MUs the signal is underdetermined, which is to say that decomposition has multiple solutions³.

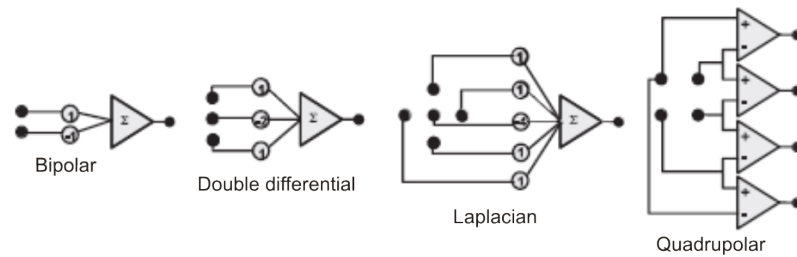


Figure 2.4 – Spatial filters are the weighted sums of various spatial arrangements of electrodes, causing high-pass filtering in the spatial domain. Adapted from Farina et al.¹⁵, ©2008, The American Physiological Society.

2.5 Multichannel sEMG

Several electrodes placed equidistance from each other (multichannel sEMG) makes it possible to study the spatial distribution of the underlying muscle and MUs⁵². An output can be derived from the voltage differential between two or more channels, with the effect of removing signal components common to each. A technique known as spatial (high-pass) filtering⁶².

2.5.1 Spatial filtering

Spatial filters are able to remove common features between both signals, which can help reduce artefact. They have the added advantage of increasing the spatial selectivity of recording, i.e. reducing cross-talk between MUs⁹. The weighted summation of the signals is performed in an amplifier stage⁴⁷. Two nearby electrodes result in bipolar recording, which is the classic configuration (or montage) for rejecting the common mode⁶². This is the simplest spatial filter and with electrodes having weighting coefficients of +1 and -1⁴⁷ (see figure 2.4). The triphasic MUAP waveform becomes quadruphasic with bipolar recording and far-field phenomena are suppressed⁶² as shown in figure 2.5.

The use of bipolar montages or higher order derivatives, such as double differential, Laplacian and quadripolar montages (see figure 2.4, considerably reduces the detection volume of each electrode, effectively diminishing the number of MUs contributing to each channel, enabling much finer discrimination⁵⁴, e.g. see figure 2.6. This is due to enhanced high-pass (spatial) filtering which suppresses the lower spatial frequencies revealing the high-frequency details within the signal. The suppression of far-field phenomena is an important consequence of all spatial filters.⁶².

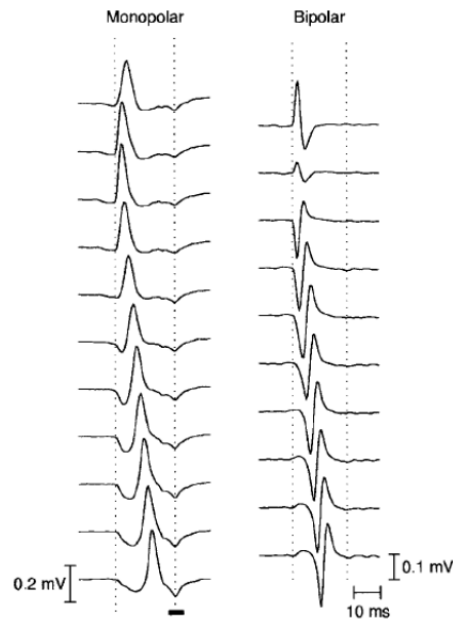


Figure 2.5 – A MUAP recorded with monopolar or bipolar montage. The dotted lines represent the location of far-field phenomena, note these are suppressed in the bipolar derivation and the waveform is altered. Figure from Zwarts et al⁶², ©2003, Wiley Periodicals.

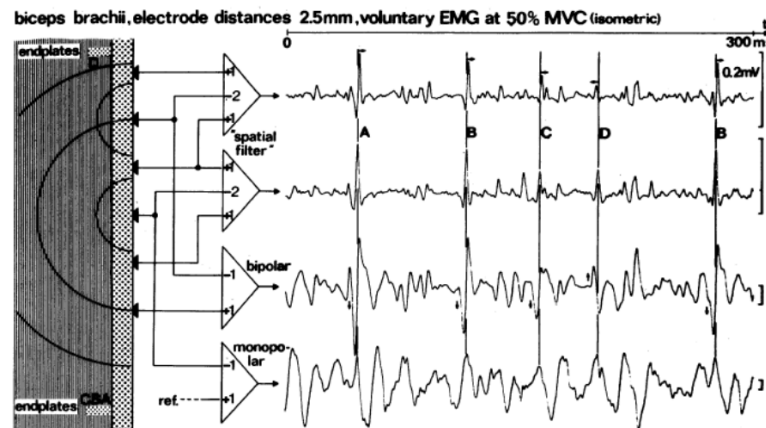


Figure 2.6 – A longitudinal array of surface electrodes with several spatial filters applied. The top two are double differential with different electrode inputs (note the inter-electrode distances remain the same). Details are enhanced with higher derivatives making MUAPs more easily identifiable. Figure from Reucher et al.⁴⁷, ©1987, IEEE.

2.5.2 The linear array

Linear arrays are multiple electrodes aligned along a single axis. They can measure the spatial differentiation of the sEMG signal in 1-dimension (figure 2.6). Due to the conservation of waveform during MUAP propagation, when applied in a direction parallel to the muscle fibres, each electrode records a signal that changes little in shape but is shifted in time. Thus, by cross-correlation, linear arrays are capable of measuring the muscle fibre conduction velocity (MFCV) of the MUAP²¹. MFCV estimation requires a linear array with a minimum of three evenly spaced electrodes⁶². The location and configuration of the neuromuscular junction has also been found with linear arrays⁴⁰. When they are aligned perpendicular to the muscle fibres they are able to capture a great deal of topographical information relating to differentiation of MUs by position, size and depth^{33 58}. More will be said on linear arrays in the following chapter.

2.5.3 The two-dimensional montage

A large disadvantage of linear arrays is that they can only offer topographical information on a single dimension⁴⁰. The expansion of electrode configuration into a second dimension can give a number of advantages, by utilising the properties of linear arrays both parallel and perpendicular to muscle fibre direction. It also allows MUs at different sites to be recorded simultaneously⁴⁹. Studies have managed to achieve results with 2-dimensional montages that were previously only within the realms of invasive techniques. For example, A cruciate arrangement of two perpendicular linear arrays, was used to detect pathologically enlarged MUs whilst accounting for depth effects⁴⁹.

2.5.4 High-density arrays

A newly developing technique within the field of sEMG uses an array of many small, equally separated electrodes inserted into a flexible medium, which allows it to conform to the contours of the surface (e.g. see figure 2.7). High-density (HD) sEMG is the subject of the next chapter where the various arrays that have been used will be discussed in detail. The main advantage of HD arrays are they have a much higher rate of spatial sampling.

2.5.5 Spatial sampling

Spatial sampling refers to the number of sampling points that occur within a given spatial period. Analogous to sampling in time, to gain adequate resolution in the spatial domain,



Figure 2.7 – An example of an early high-density sEMG array as developed by Blok et al.² ©2002, American Institute of Physics.

the density of the electrodes must meet the spatial version of the Nyquist criterion². Two of the defining parameters of a HD array are, therefore, the inter-electrode distance (IED) and electrode diameter as these dictate the spatial sampling rate⁴¹. Examples of these are given in chapter 3, tables 3.2 and 3.3.

For accurate sEMG detection, it is suggested that (for the direction parallel to muscle fibres) a maximum IED of 5 mm should be adhered to in order to meet the spatial Nyquist criterion. This is based on a temporal Nyquist limit of 800 Hz (see section 2.3.2) and a muscle fibre conduction velocity (MFCV) of 4 m/s². As electrode size decreases however, the electrode-skin impedance will, unfortunately, increase². Several methods of overcoming this have been attempted, as will be discussed in the following chapter.

2.6 Summary

This chapter has introduced the concept of surface electromyography. In order for the challenges faced by this technique to be appreciated, the physiology of the motor units were discussed. Different configurations of surface electrodes were discussed, the most advanced of which is the high density array. This is the subject of the next chapter which aims to give a systematic view of the available literature. In order to appreciate the technicalities of design the concepts of spatial filtering, spatial sampling and spatial selectivity were introduced.

Chapter 3

High-Density Surface Electromyography: a review of the literature so far

3.1 Introduction

As the title to the chapter suggests this section will be a literature review surrounding the use of high-density surface electromyography (HD sEMG). HD sEMG has been discussed in detail in the previous chapter (see chapter 2 section). For this study I will be referring to the use of a two-dimensional (2D) array of electrodes with high spatial density. Generally I have limited this review to studies using more than two electrodes in each dimension as these are more relevant to my own research. However, where necessary for clarity, studies using linear arrays, having a single column of monopolar or bipolar (i.e. two columns of monopolar) electrodes may be mentioned. As a further note, many of the terms referred to within this chapter are defined in the Glossary (Appendix I).

3.1.1 Span of the field

This is a relatively recent technology. Although first applied by Masuda et al. in 1988⁴⁰ it did not really take off in terms of research until the new millennium. A timeline of the literature is shown in table 3.1. Due to such brevity I am in the fortunate position of being able to review the majority of research completed in this field. As the timeline shows, I was able to find about 30 papers on HD sEMG, dating from 1988 to the present. These were found by searching for

studies and reviews concerning HD sEMG on various search engines (most noticeably ISI Web of Knowledge and Google Scholar), examining those which were referred to in other papers and by searching for papers citing references to HD sEMG studies. Keywords used were 'high-density' or 'HD' combined with either 'surface electromyography', 'surface EMG' or 'sEMG'. Note that these search engines are not case sensitive. The inclusion of other words, such as 'multichannel' included too many false-positive results pertaining to sub-HD techniques. The majority of studies relate to the application of HD sEMG to pre-existing problems. There are also several reviews with some mention of HD sEMG which have also been included.

3.1.2 Review structure

The first section of this review will provide general information on HD sEMG. The experimental setups have been summarized, along with electrode array specifications, recording parameters and muscles used in tables 3.2 and 3.3. The second section will therefore discuss the HD electrode arrays that have been used.

In the penultimate sections, the studies will be broadly categorised in terms of experimental aim. Within these, they will be subcategorised by signal analysis technique and method of validation. Due to the number of different applications to which HD sEMG has been applied, categorization is not very clear cut, meaning many studies fall into more than one category. As this is a very new and rapidly advancing field, methodological validity will be an overriding theme of this review.

3.1.3 Research groups

Two major research supergroups feature prominently in the literature, within which occurs much co-authoring and sharing of hardware and techniques. Reference to these research syndicates enables me to subcategorise the relevant literature in an alternative way where appropriate.

The first group, based largely in the Institute of Neurology, part of the University Medical Centre Nijmegen, in The Netherlands, most noticeably includes Kleine, Blok, Stegeman, Zwarts, van Dijk, Roeleveld, Drost and Lapatki, each of whom have authored and co-authored many papers relating to sEMG. This group (of which I will refer to as the 'Dutch research syndicate') is largely composed of researchers with medical backgrounds and this is represented in their techniques which require a high level of knowledge of MU physiology.

The second group is largely focussed around the Laboratory for Engineering of the Neuromuscular system (LISiN) at Politecnico di Torino in Italy. Most noticeably it includes Merletti,

Farina, Holobar, Zazula and Gazzoni. The members of this group (of which I will refer to as the 'Italian research syndicate') largely come from engineering backgrounds which is represented in their more mathematically complex, fully automated approach.

3.2 Challenges of HD sEMG

This section will discuss the advantages that HD sEMG offers over more conventional forms of sEMG. Following this it will explain some of the concepts necessary for an understanding of this review, these are: the interference signal and the importance of validating results. The interference signal was discussed in chapter 2, therefore only brief recapitulation is necessary.

3.2.1 Advantages

Every paper on the subject extols the virtues of HD sEMG, so it is not hard to find the hypothetical advantages. The most obvious advantage is the non-invasive nature, which makes it much more suitable for use on children and athletes than intramuscular electromyography (iEMG)¹⁵. There may also be the additional advantage of being able to safely measure stronger contractions without risk of tissue damage^{15;18}. Unlike iEMG it is possible to reproduce the same results in subsequent studies with HD sEMG³⁹ giving a large advantage to long term studies and assessment. The detection volume, i.e. the area of tissue within range of the electrodes, is much larger than conventional sEMG or iEMG. This causes more motor units (MUs), the functional unit of muscular activation, and muscle fibres are observable. A further consequence of this is the addition of topographical information which can be extracted. These spatial advantages will be discussed in more detail later.

3.2.2 The interference signal

HD sEMG has been used for many purposes, as table 3.1 shows. However, the 'philosopher's stone' of sEMG, that which more effort has been channelled towards than any other, is the extraction of individual MU contributions from the surface recorded signal.

The sEMG signal is composed of many different MU contributions, and unfortunately noise, which are superimposed upon each other resulting in constructive and destructive interference. These processes therefore result in loss of information in the surface recorded 'interference' signal, as discussed in chapter 2. The problem is compounded by the high-pass filtering effect of the tissues between the MUs and the surface which causes MUAPs to appear more similar. Fortunately, spatial information gained from multiple recording sites, using HD sEMG, can

be used to resolve superimpositions and thus extract individual MU components from the interference signal³³, a process termed decomposition. Although this refers to the extraction of MUAPs from any signal, in this review it will specifically imply HD sEMG decomposition, unless otherwise stated. A large portion of this review and previous reviews on HD sEMG have been devoted to this subject.

3.2.3 Validation of results

Any system hoping to further scientific knowledge must be able to prove, beyond reasonable doubt, that its results are legitimate. Confidence must be inferred through scientific methodology. Many of the studies reviewed try to validate their techniques through the use of experimental clues, by using computer simulations and by comparison of results with those of other techniques. Results can be evaluated with respect to known parameters of the underlying physiology to gain some clue as to their validity. The input values are unknown so concrete evidence is impossible. Only indirect measures are achievable, most of which are subjective and qualitative at best. By comparing results to literature values, a rough estimate of accuracy can be obtained. Such an analysis can only be regarded as qualitative.

A knowledge of the underlying physiology can be used to predict the transfer functions between MU firings and surface recordings, allowing systems to be modelled *in silico*. This is a very popular method of validation on the subject, especially from the Italian research syndicate. Unfortunately it is very difficult to estimate the relevance of such results to real scenarios, especially as emerging patterns seem to be less definite when the same algorithm is applied to real signals²⁶. Whilst none of these methods is infallible, the inclusion of two or more modes of validation creates a high level of verisimilitude in the accuracy of the results.

3.3 Existing Reviews

As mentioned there are several reviews which touch upon HD sEMG already in existence. Roeleveld and Stegeman⁵⁰ provide an insightful review of how sEMG (noticeably HD sEMG) has led to a increased understanding of MUs. As the authors are both affiliated with the Dutch research syndicate, discussion of such is mainly limited to studies using the device designed within the group by Blok et al.^{2;10;33;35;36;34}. Mention of the arrays predating this by Masuda & Sadoyama⁴⁰ and Pruchi⁴⁶ are curiously absent. However, a more comprehensive review by Zwarts et al.⁶² (also part of the Dutch syndicate), just one year later, does make mention of these previous HD arrays, although the focus still lies primarily with the Blok et al. version. Both of these, relatively similar, studies provide details on the application of this array to signal

decomposition. An area previously thought possible only through intramuscular EMG (iEMG). The remaining two reviews are much more recent and, interestingly, both by members of the Italian research syndicate. The first, in 2008, is by Merletti et al.⁴¹ and gives by far the most in-depth review of decomposition techniques using HD arrays. A distinction is made between partial and complete decomposition. Complete decomposition requires that all MUs contributing are isolated with every firing instance accounted for. Muscle fibre membrane properties which can be estimated with partial decomposition are discussed. However, it strongly suggests that complete decomposition be attempted as knowledge of MU behaviour can augment such muscle fibre properties enabling the study of neural and muscular adjustments in MU properties. Mention is also made of the various techniques that have been applied to the decomposition problem in which blind-source techniques, whereby the underlying physiology of the MU is ignored, are advocated. The latest review by Farina¹⁴ is largely concerned with the problems that can arise with using sEMG signal amplitude to infer details of neural activation. It is suggested that changes in MU firing behaviour correlate much more accurately with neural drive. Of course, complete decomposition is required for inference to be meaningful.

3.4 HD array design

As discussed in chapter 2, HD sEMG is specified by the electrode configuration. This section discusses how the parameters of the array affect performance. Many of the concepts that were introduced in the previous chapter are used within the section.

3.4.1 Number of channels

That which elevates HD sEMG above other forms of electromyography is the huge number of 'vantage points' (i.e. channels) by which the signal can be observed. More electrodes therefore decrease the likelihood that two different MUs have the same sEMG representation. The use of multiple electrodes, as discussed in the previous chapter, also increases spatial sampling and spatial filtering.

3.4.2 Spatial sampling

Spatial sampling determines the degree to which spatially distributive features can be segmented (the spatial sampling frequency). Analogous to temporal sampling frequency it is inversely proportional to the interelectrode distance (IED).

3.4.3 Spatial filtering

The use of bipolar or higher derivative montages (see chapter 2 section) increases the spatial selectivity of each electrode, effectively diminishing the detection volume (i.e. the number of MUs contributing to each channel), enabling much finer discrimination⁵⁴. It is this spatiotemporal information which allows decomposition of surface potentials.

3.4.4 Spatial density

From this it would seem that a smaller IED is preferable. Unfortunately increasing the spatial density must either result in a smaller total detection area, thus losing global topographical information of the muscle, or more electrodes, creating an exponentially large dataset. Tables 3.2 and 3.3 show that the most common IED used is 5 mm.

The array specifications must be appropriate for the task and studies generally settle on a compromise between size and density. Masuda and Sadoyama⁴⁰ found that an IED of 2.54 mm was able to give vastly superior results to the analysis of innervation zone location and configuration over previous research. They posit that solid electrodes are required for such a high spatial density.

3.4.5 Array size

Array sizes can vary dramatically, from the relatively massive 256 channels used by Pruchi⁴⁶ to the comparatively tiny 16 channels of García et al.¹⁸. Interestingly the earlier arrays are predominantly larger than more recent designs (see tables 3.2 and 3.3). The Dutch and Italian research syndicates seem to have their own preferences.

The use of a 2D array allows the selection of channels with the highest signal-to-noise ratio (SNR), a 'go where the action is' approach³⁸. Many studies, such as the decomposition techniques of Kleine et al.^{33;35;36;34}, limit the number of channels used to process the signal, in order to reduce the complexity of the task, to a single (bipolar) column (parallel to muscle fibres) or row (perpendicular to muscle fibres).

Due to the conservation of charge during propagation, a column of channels aligned with the muscle fibres (columns) will produce a very similar profile but with a latency inversely proportional to the muscle fibre conduction velocity (MFCV). Some studies have exploited this fact to calculate the MFCV using cross-correlation values between channels within a row (perpendicular to muscle fibres)^{10;13;21;46}. It was found that a single row can supply most of the topographical information relating to differentiation of MUs by position, size and depth^{33;58}.

Kleine et al.³⁵ found that use of single (bipolar) rows gave very little performance loss, for decomposition, when compared to use of all channels. The same experiment found that single columns resulted in significant performance deterioration.

3.4.6 Attachment

One major limitation of the older arrays (pre-2004) was the method of attachment. Most were secured by some sort of strap, producing uneven contact and allowing slight changes of electrode position. Thus a significant improvement to array design was the self-adhesive aspect of Lapatki et al.³⁸, a feature that was quickly incorporated into other studies, e.g. Grönlund et al.²¹, Holobar et al.²⁴). The downside of adhesive arrays is that adjustment of position is impossible after attachment³⁸.

3.4.7 Electrode size

Higher density requires a significantly reduced area size compared to sEMG. The advantage of using small electrodes is greater spatial filtering, thus fewer MUs contributing to the interference signal^{54;42}. The disadvantages include weaker signals and higher impedance. It is suggested that the use of an adhesive array with gel-filled cavities provides much lower electrode-to-skin impedance¹⁵. This design is limited, however, to fairly large IEDs usually of about 8 mm. Blok et al.² sought to overcome this problem by using serrated (electrode) contact surfaces, thus increasing the surface area of contact without altering the detection area. Some studies (e.g. Masuda & Sodayama⁴⁰) applied electro-conductive paste to the skin before recording. Unfortunately this can increase the likelihood of shorting between electrodes. Prutchi⁴⁶ incorporated a buffering system which enabled impedance control of individual channels.

3.5 Decomposition techniques

This section will discuss the various attempts that have been made to decompose the sEMG signal using a HD array. The difficulties will be discussed and a common technique called spike-triggered averaging will be mentioned. The decompositions will be divided into fully automated algorithms and those that require interaction. The section will finish with a discussion into methods that have been used to try and validate techniques.

3.5.1 Difficulties

To recap, decomposition refers to the resolution of the EMG interference signal to the individual MUAP contributions and their identification with respect to underlying MUs²⁷. This is complicated by the underdetermined nature of the signal. The constructive and destructive nature of superimpositions create a very large set of possible solutions to Laplace's equation for a bounded inhomogeneous medium, given only surface potentials⁵⁸. As stated previously, the spatial extension of data from a 2D array can help to reduce the number of solutions.

3.5.2 Spike-triggered averaging

MUAP extraction is usually undertaken by spike-triggered averaging^{33;35;36;34}, in which an averaged response to a stimulus is taken which can be used to locate future responses (Farina et al. 2008). This technique relies on the following assumptions³²:

1. The delay between trigger and response is fixed
2. The response is independent of other signals.
3. The response waveform is conserved.
4. There are sufficient trigger events to extract a representative response.

Unfortunately, when applied to sEMG, some of these assumptions may be violated during temporary synchronization of MUs³² or from feedback inhibition within the spinal cord²³. This has consequences on the accuracy of estimations of MU properties based on sEMG features extracted using spike-triggered averaging. In the following decomposition techniques, the assumption of waveform conservation is extended. For decomposition to be at all possible it is assumed that surface potentials from the same source show less variance than those of different sources.

3.5.3 Interactive techniques

Classification of decomposition techniques leads to the very broad divide, into those requiring interaction by the operator and those which have automated algorithms, which tends to reflect the backgrounds of the researchers. Most noticeably those affiliated with the Dutch research syndicate tend to favour interactive techniques, where medical knowledge must be applied to the decomposition process, and those affiliated with the Italian research syndicate tend to strive towards a fully-automated process, making the technique accessible to the inexperienced.

Template matching is a technique used extensively in iEMG decomposition. It involves the sequential detection of action potentials from the signal which are classified in accordance to their waveform similarity. Those within specified similarity limits are viewed as temporally separated firings of the same MU. When this technique is applied to HD arrays it must take account of waveform and time differences of the same MUAP in different channels. Whilst increasing computational costs, such spatiotemporal variation compensates in some way for the removal of waveform detail as signals radiate through the tissues. A HD sEMG template matching technique was developed by Kleine et al.³³ and used in many subsequent studies by affiliates of the Dutch research syndicate^{2;11;35;36;34;38}.

The template construction procedure consists of the following stages: peak detection, clustering and spike triggered averaging, with many opportunities for manual adjustment. The paper by Kleine et al. from 2007 gives the most detail into these stages: Initially, a single row of channels is chosen at the operators discretion, based largely on SNR and likely superimpositions. Peaks are detected automatically but the threshold for a peak is specified by the user. Thus experience of sEMG signals can help separate MUAPs from noise. Next, an algorithm, based on Wards clustering, groups peaks by waveform similarity until a user defined number of groups remains. The number of groups is based on an estimation of the probable MU population contributing to the signal. The results are displayed as histograms of the inter-spike intervals (ISI) and knowledge of physiologically probable firing behaviour is applied by the user to merge, split or delete clusters as appropriate. Clusters are then used to form templates in these channels. Spike-triggered averaging is used to define MUAP firing times and the templates are expanded to include all channels. Channels are inspected visually and those of poor quality are excluded. Multichannel MUAP templates are sequentially subtracted from each sampling point in a peel off procedure. Subtractions giving maximal signal reduction are assumed to correlate to a firing instance and the subtraction is saved. An advantage of this approach is that subtraction of an MUAP from a complex waveform (i.e. a superimposition) could reveal the presence of a smaller MUAP. This occurs for every template though the entire signal until subsequent iterations bring no further signal reduction. Finally, the signal is reconstructed from the templates and firing instances and is cross-correlated with the interference signal for validation. More will be said on validation later.

When the number of active MUs was kept low this seemed able to decompose as much as 97% of the interference signal³³. That is to say that 97% of the MUAPs identified were matched to a MU. However, sporadically firing MUs, such as from one at the lower-limit of its recruitment range, would preclude the generation of a template and be viewed as signal artefact. Similarly, low amplitude MUAPs were indistinguishable from background noise. As the highest amplitude MUAPs were subtracted first, a slight bias towards these was reported³⁵.

3.5.4 Automatic techniques

There appear to be two studies which have developed entirely automated template-matching techniques. Gazzoni et al.¹⁹ uses template matching for HD sEMG decomposition. It should be noted that Gazzoni is heavily affiliated with the Italian research syndicate and this appears to represent the groups first attempt at decomposition using HD arrays. Possibly reflecting the groups less clinical background this is an automatic procedure. Wavelet analysis was used to select candidate templates whilst multi-channel Adaptive Resonance Theory (MART) artificial neural networks (ANN), consisting of a set of parallel ART2 neural networks (one per channel), allowed for spatial variation in the templates. This technique had limited application, however, as it was unable to resolve superimpositions.

The techniques mentioned so far rely on *a priori* information regarding the underlying physiology of MUAPs. However, by exploiting another of the assumptions of spike-triggered averaging, this information can be ignored. Or at least that is the theory behind blind-source separation (or blind-identification) which assumes that firings from individual motor units are statistically independent of each other and that signals are stationary. No assumptions about firing behaviour are made, thus sporadic MUAPs can also be detected⁴¹.

García et al.¹⁸ developed a blind-identification algorithm, based upon independent component analysis (ICA), to create the templates. ICA uses the most significant eigenvectors of the dataset to find the features of most important variance. In simulations independent components correlated well with firings from different MUs. However it was limited in that it did not account for spatial differentiation⁴¹.

Holobar and Zazula²⁶ modelled the interference signal as a mixture of linear time-invariant (LTI) responses in a multiple-input-multiple-output (MIMO) system. By filtering the signal through an inverse correlation matrix, resolution of the convolutive effect of volume conduction is attempted. Results from simulations implied noise resistance and an ability to resolve superimpositions and short-term MU synchronicity. Based upon this model, the convolution kernel compensation (CKC) method of decomposition was developed^{24;25;27}. It does not attempt to identify the underlying convolutive transfer function thus reducing the computational burden of the previous method⁴¹. It assumes that the firings of any particular MU are sufficiently sparse that any synchronization is likely to be transitory²⁷. Using this method on a number of subjects the discharge patterns of up to 20 MUs were automatically identified²⁴. In simulations, identification probability was determined largely by surface energy. That is, small or deep MUs were considered noise. Simulations also showed that MUs which were at their lower limit for recruitment, and therefore contributed only a few peaks to the sEMG signal, were considered signal artefact. The limits of active MU pool size were also simulated. Higher forces

increase the probability of transient synchronicity between MUs as more MUs become active and firing rates increase. Transient MU synchronicity, could result in a false template, however, precluding the application to higher forces²⁵. It is quite interesting that these seem to be the chief sensitivity problems of the interactive technique of Kleine et al.²⁷, suggesting that these are limitations to HD sEMG decomposition in general rather than to specific techniques.

3.5.5 Validation of results

One of the main reasons for the slow uptake of HD sEMG into clinical usage for MU analysis is the lack of performance validation²⁴. As previously discussed several studies make subjective estimates of their reliability, based on knowledge of the underlying physiological parameters. Kleine et al.³⁴ suggest clues on the completeness of firings resolved, the regularity of firings and MUAP waveforms. Holobar et al.²⁴ made similar assumptions, looking at linearity of recruitment and derecruitment thresholds (using ramped force), the discharge rates at these thresholds, and the amount of signal energy accounted for by identified MUAPs (the signal to interference ratio, SIR). It was also noted that the number of MUs identified remained the same during repeats for every muscle investigated.

Kleine et al., looked at interoperator agreement³⁶, to see if the subjective nature of interactive techniques limited performance. Two novices were given identical training in the technique (see Kleine et al.³³) and asked to independently decompose the same raw data (from Kleine et al.³⁵). Despite a tolerance of 2ms on firing instances, complete agreement occurred on only around 35% of MUAPs. Agreement was however quite high (the majority being in 90-100% agreement) for fully decomposed MUAPs. It was felt that this gave a good upper limit on decomposition performance. The possible flaw in this line of reasoning is that the authors have presumed that agreement on results is proof of accuracy. In fact this is only proof of precision (i.e. reproducibility). They do not seem to have considered that intrinsic errors could render the algorithm incapable of achieving correct results.

A major hindrance to performance validation is the lack of a gold standard for HD sEMG decomposition³³. This is not the case with iEMG, the gold standard for which is generally assumed to be the 1954 method of Buchthal et al.³⁶. Direct comparison to this more clinically accepted method has been used as a means of evaluating reliability. Holobar et al.,^{24;25} recorded concurrent iEMG with HD sEMG, using the EMGLAB decomposition tool developed by McGill et al. (2005) to decompose the iEMG signal interactively. It was found that the methods tended to identify different pools of MUs. Despite this, the match between firing instances of those identified with iEMG and sEMG (with a tolerance of 0.5 ms) was as high as a 98%²⁴. The study was later extended to include more muscles²⁵. Again, different techniques revealed different MU pools. The average agreement on those simultaneously identified ranged from 84% in the

biceps brachii to 92% in the abductor digiti minimi. This high agreement on firing patterns gives heavy credence to these being accurate representations of MU behaviour, especially considering the tried-and-tested nature of iEMG. A discussion into the validity of this interactive, and thus subjective, approach, however, is beyond the scope of this review.

A number of the automatic decomposition techniques were tested with simulated sEMG recording^{15;19;24;25;27;26}. As the solution is actually known the algorithm can be directly verified, however the degree to which these techniques can apply to real situations introduces another source of uncertainty.

3.6 Other experimental aims

3.6.1 Motor unit number estimation

Using the same clustering technique of Kleine et al.³³, but without the complete decomposition procedure, van Dijk et al.⁵⁴ used the spatiotemporal properties of a HD array to alleviate the problems of alternation during motor unit number estimation (MUNE). See tables 3.2 and 3.3 for details. MUNE involved the sequential increase of muscular activation, through external stimulation, to infer the total MU population size from the recruitment curve. This was based upon the incremental counting technique of McComas described in 1971 (van Dijk et al.⁵⁴). Alternation occurs when MUs have an activation threshold very close to the stimulation level and so will 'alternate' between a state of activation and inhibition. They posit that the difference in shape between the mean MUAP and the compound muscle action potential can give a quantitative assessment of validity. Such comparison showed that some MUAP profiles were under or over represented in the MUNE, thus the value obtained may not be truly representative of the entire MU population.

3.6.2 Topographical information

Where HD sEMG excels over other forms of EMG is in the amount of topographical information that can be obtained fairly simply. The innervation zone is the area where the motor-neuron synapses with the muscle fibres. All MUAPs originate from these structures. Please refer to the previous chapter for a more detailed description. By using HD sEMG to locate MUAP foci, Masuda & Sodoyama⁴⁰ found that around 70% of MUs had only a single innervation zone region, whilst some had more complex patterns. They estimated that the length of innervation zones along the muscle fibres was as much as 60 mm over the whole muscle, a finding that agrees with histological studies by Aquilonius et al. However, their findings suggest the innervation

zone of individual motor units to be much longer than histological studies by Co'ørers and Telerman-Toppet had predicted. Much more recently Guzmán et al.²² used a HD array to find the IZ location and adjusted this for anatomical variation. They assumed validity based on agreement with the results of another recent study (exact figures not specified).

3.6.3 Prosthetic control

An approximation of HD sEMG has been applied to the field of prosthetic control by Zhou et al.⁶¹ and Huang et al.³⁰ These did not use what I have defined as a true HD array, rather an extremely large number of single channel electrodes arranged in a 2D grid. As a result the IED was quite high and not fixed. Targeted muscle reinnervation involves rerouting peripheral motor nerves for an amputated limb to a now-redundant muscle, using the muscle as a natural amplifier. EMG controlled prosthetic limbs using this muscle gained a much more useful method of control⁶¹. Following on from this study, an algorithm was developed to extract an optimal configuration of electrodes which could provide a similar quality of control but with considerably fewer electrodes. They found that 11 electrodes arranged in a configuration determined by the algorithm could differentiate 16 movement commands with 93% accuracy on average, or 77-87% accuracy with just 5 electrodes. It was also found that arrangements based upon anatomical heuristics, making it much more accessible to clinicians³⁰, performed only 4.3% worse.

3.6.4 Propagation

MUAPs should propagate along the muscle fibre with spatiotemporal stability. (See previous chapter for more information). Changes in propagation properties can thus be important factors in assessment of neuromuscular disorders. Of particular clinical usefulness is the conduction velocity along the muscle fibre. After decomposition this constitutes second most common line of research with HD sEMG. In fact, the second study using a 2D HD array was the development of a system to automatically detect the MFCV⁴⁶, the results of which were comparable to literature values. This was a very sophisticated design, but the design was not taken up by other researchers.

One of the problems of calculating MFCV with electrodes arrays is that that misalignment of the column with the muscle fibre will lead to an overestimation in distance travelled by the MUAPs and thus in propagation velocity. Not only this but fibres not parallel to the surface will have a similar effect. Gr'ønlund et al.²¹ developed a technique to accommodate for this by first estimating the muscle fibre orientation relative to the electrode alignment. This relied on linear least absolute deviation regression to fit a 3D function to each MUAP, using amplitude for an estimate of depth. It assumed that amplitudes were monotonic and above background

noise and MFCV was constant. The algorithm was largely tested on simulated signals. It appeared able to differentiate individual MUs, from a very low pool, based on their MFCV. However, due to the lack of a dedicated decomposition function, estimates tended to degenerate when many MUs were active. Validation was carried out through simulation and comparison with a visually based estimation of the underlying muscle fibre orientation.

The spatiotemporal properties of HD arrays were exploited to look at how MFCV can vary locally in time and globally in space by Farina & Fala¹³. This was the only study using dynamic movements and hoped to track MFCV changes resulting from fatigue. The extra channels reduced variability of the estimates allowing smaller changes to be identified. The accuracy was estimated from the standard deviation of residuals from a regression line fit to the data.

3.7 Conclusion

The literature on HD sEMG was discussed. In doing so the advantages of using the a HD array were explored. This topic was chosen for review as my own research involved HD sEMG. In order to fully understanding of the techniques involved new concepts were defined and previously defined terms were reiterated. There was a strong distinction between procedures that aimed to be fully automated and those that required manual interaction. Such a choice would have ramifications on the feasibility of application of the technique into a clinical setting, where training may be necessary if operator skill is required. Two major research groups have emerged. One, with members of largely medical backgrounds, appears to favour an interactive approach, whereas the other, composed mainly of engineers, seems to favour automated techniques.

Despite the obvious potential of HD sEMG it has yet to make the transition into regular clinical practice. The reasons for this relate to the difficulty in validating the results, the lack of a gold standard to compare performance against is a large factor in this. Validation was thus a strong theme of this chapter. Validation was either through computer simulation, the physiological relevance of the procedure or comparison to known parameters of results from a simultaneous experiment with different techniques. Evidence for accuracy is higher in those experiments which use multiple methods of validation. The relative costs of HD arrays and the multichannel amplifiers needed to process the signals were not mentioned in any of the papers, however some reference was made to the technical expertise necessary for its application.

Table 3.1 – A timeline of the literature. Shaded rows denote literature reviews.

Date	Authors	Brief summary of study
1988	Masuda \& Sadoyama	Design of the first HD array which was applied to the characterization of muscle fibre IZs.
1995	Pruchi	Design of state-of-the-art HD array and algorithms to calculate MFCV.
2000	Kleine et al.	Use of HD sEMG to extract magnetic stimulation-induced MU firings using an interactive template-matching and sequential subtraction algorithm.
2001	Wood et al.	Use of Linear (bipolar) array and FEA to investigate MU property changes in motor neuron disease patients
2001	Drost et al.	Application of HD array to the characterization of MUAPs in patients with generalized myotonia (Becker's disease) displaying transient paresis
2002	Blok et al.	Design of a novel HD array, with limited flexibility, using metal pins on a foam block to extract and characterise individual MUAPs. Note this is the array used by Kleine (2000) and Drost (2001).
2002	Roeleveld \& Stegeman	A review of MUAP underlying physiology and how they can be extracted using sEMG. Mention is made of some of the HD studies so far.
2003	Zwarts et al.	A review of sEMG with a large section devoted to studies using the array designed by Blok (2002).
2004	Drost et al.	Application of HD array to characterise MU changes in postpoliomyelitis syndrome patients, using decomposition technique of Kleine (2000).
2004	Gazzoni et al.	An automatic system for sEMG signal segmentation and MU identification based on CWT and modified MART ANN.
2004	Holobar \& Zazula	A novel, correlation-based, blind-source decomposition algorithm was designed and tested on real and simulated sEMG signals.
2004	Lapatki et al.	Design of a new flexible, adhesive HD array for extraction of facial MUAPs.
2005	Garcia et al.	A blind-source decomposition algorithm using template-matching and ICA to investigate large voluntary contractions.
2005	Grönhund et al.	An algorithm to simultaneously estimate MFCV and muscle fibre orientation using a HD array to compensate for suboptimal electrode alignment.
2005	Zhou et al.	Use of a semi-HD array to aid prosthetic control after targeted muscle reinnervation
2007	Holobar \& Zazula	A new, blind-source algorithm for MUAP decomposition using convolution kernel compensation.
2007	Kleine et al.	Use of previous technique (Kleine, 2000 and Drost, 2004) to extract MUAPs using the HD array designed by Blok (2002), with more detail on implementation and interpretation.
2008	Van Dijk et al.	Use of a HD array (Lapatki 2004) to counteract alternation problem when estimating number of motor units within a detection volume
2008	Farina \& Fala	Use of a HD array to estimate MFCV changes within muscle fibres using a maximum likelihood estimator.
2008	Huang et al.	Continuation of targeted muscle reinnervation study by Zhou (2005) using (semi) HD sEMG on four amputees to improve prosthetic control.
2008	Kleine et al.	To validate the decomposition technique (Kleine 2000, 2007), 2 new operators were trained and their results compared for similarity.
2008	Kleine et al.	A case report on the use of HD sEMG to investigate the effects of neuromyotonia (Isaacs' syndrome) on firing behaviour.
2008	Maathuis et al.	A look at the feasibility of the long-term tracking of MU changes with HD sEMG.
2008	Merletti et al.	A review of HD decomposition techniques developed so far, with a strong emphasis on blind-source decomposition techniques.
2008	Farina et al.	An investigation into the effects of channel number and spatial filter type on decomposition, through simulation and experiments with concurrent iEMG.
2009	Holobar et al.	A validation of a previous algorithm (Holobar \& Zazula, 2007) though simulated and real HD sEMG experiments, one with concurrent iEMG.
2009	Lapatki et al.	Use of a HD array to measure toxin diffusion following therapeutic injection of botulinum toxin.
2010	Farina et al.	A review of the relationship between sEMG signal amplitude and neural activation. Some mention of using MU firing behaviour by HD sEMG.
2010	Holobar et al.	Comparison of HD sEMG decompositon algorithm with iEMG as in 2009 but in more depth and with more trials.
2011	Guzmán et al.	Use of a HD array to characterise IZ to find the optimal injection site of botulinum toxin.

Table 3.2 – The experimental parameters used within this review, part 1

Study	Main aim	Electrodes	Array	Recording	Muscles	Contraction	Trials
Masuda et al. (1988)	IZ configuration	Solid	Size: 9x14 IED: 2.54x5.08 mm d : area = 0.4 mm ²	BW: 350-1600 Hz Gain: 63 dB f_{amp} : 4094 Hz	Biceps brachii	Voluntary <20% MVC Visual feedback	Subjects: 3 Repeats: N/S
Prutchi et al. (1994)	MFVC (range)	Solid	Size: 32x8 IED: N/S d : ?	BW: 1 kHz? Gain: Adaptive f_{amp} : ? Hz	Biceps brachii	Voluntary 100% MVC	Subjects: 1 Repeats: 4
Kleine et al. (2000)	Decomposition	Solid	Size: 13x10, IED: 5 mm d : 1.52 mm	BW: 3-400 Gain: 153 f_{amp} : 2000 Hz	Biceps brachii	TMS 5% MVC Visual feedback	Subjects: 5 Repeats: 100
Kleine et al. (2007)					Vastus lateralis	Voluntary Ramp: 0-5% MVC	Subjects: 1 Repeats: N/S
Kleine et al. (2008a)					Gastrocnemius	N/S	Subjects: 1 Repeats: 1
Kleine et al. (2008b)					N/A	N/A	Subjects: N/A Repeats: N/A
Blok et al. (2002)					Array design		
Drost et al. (2001)	MUAP propagation			BW: 3-400 Hz Gain: N/S f_{amp} : 2000 Hz	Biceps brachii	Voluntary 5-100% MVC	Subjects: 7 Repeats: 1
Drost et al. (2004)	Decomposition and MU characterization				Vastus lateralis	Voluntary 5-100% MVC	Subjects: 18 Repeats: 3
Grönlund et al. (2005)	MFCV and MFO			BW: N/S Gain: N/S f_{amp} : 2048 Hz	Biceps brachii	Voluntary 5% MVC	Subjects: 2 Repeats: N/S
Wood et al. (2001)	MU characterization	N/S	Size: 16x2 IED: 5x3 mm d : ?	BW: 12-2500 Hz Gain: 15000 f_{amp} : 5 kHz	Flexor digitoralis superficialis	Moderate Steady Voluntary	Subjects: 22 Repeats: N/S
Gazzoni et al. (2004)	Decomposition	N/S	Size: 61 IED: 5 mm d : N/S	BW: 10-500 Hz Gain: N/S f_{amp} : 2048 Hz	Biceps brachii	5% MVC	Subjects: N/S Repeats: N/S
Lapatlá et al. (2004)	Array design and decomposition	Gel-filled cavity	Size: 7x13 IED: 4 mm d : 1.2 mm	BW: 3.2-400 Hz Gain: N/S f_{amp} : 7Hz	Upper face Lower face	N/S Visual feedback	Subjects: 13 Repeats: N/S

Table 3.3 – The experimental parameters used within this review, part 2

Maathius et al. (2008)	Decomposition and MU tracking	Gel-filled cavity	Size: 14x9 IED: 4 mm d : 1.5 mm	BW: N/S Gain: N/S f_{amp} : 4096 Hz	Abductor pollicis brevis	TES	Subjects: 10 Repeats: 4
Farina \& Fala (2008)	MFCV		Size: 13x5 IED: 8 mm d : 1 mm	BW: 10-500 Hz Gain: 5000 f_{amp} : 2048 Hz	Biceps brachii	Dynamic Maximal speed	Subjects: 4 Repeats: 1
Holobar et al. (2004)	Decomposition		Size: 13x5 IED: 5 mm d : 1 mm	BW: 10-500 Hz Gain: 10000 f_{amp} : 2048 Hz	Biceps brachii	Voluntary 5 and 10% MVC Visual feedback	Subjects: 5 Repeats: N/S
Holobar et al. (2009)	Decomposition	Solid	Size: 13x5 \& 12x5 IED: 2.5 \& 5 mm d : 1 \& 2 mm	BW: 10-500 Hz Gain: N/S f_{amp} : 1650 Hz	Numerous	Voluntary ramp 0-10% MVC Visual feedback	Subjects: 2-8 Repeats: 5
Holobar et al. (2010)	Decomposition		Size: 16 IED: 2.54 mm d : 1 mm	BW: 10-500 Hz Gain: N f_{amp} : 2048 Hz	Biceps brachii Tibialis anterior Abd. dig. minimi	Voluntary 5-20% MVC Visual feedback	Subjects: 12 Repeats: 3
Garcia et al. (2005)	Decomposition	Solid	Size: 15x8 IED: 4 mm d : 1.5 mm	BW: 70-1000 Hz Gain: 80 dB f_{amp} : 10 kHz	Biceps brachii	Voluntary 5-60% MVC Visual feedback	Subjects: 8 Repeats: 5
Van Dijk et al. (2008)	MUNE	Solid	Size: x ? IED: ? mm d : ? mm	BW: 0.16-400 Hz Gain: N/S f_{amp} : 2048 Hz	Thenar muscles	TES	Subjects: 14 Repeats: >4
Huang et al. (2008)	Prosthetic control	Solid	Size: 7x7 IED: 2.5 mm d : 1 mm	BW: ? Hz Gain: ? f_{amp} : ? Hz	N/A (TMR)		Subjects: ? Repeats: ?
Farina et al. (2008)	Decomposition parameterization	N/S	Size: 13x5 IED: 8 mm d : 2 mm	BW: ? 10-500 Hz Gain: N/S f_{amp} : ? 2048 Hz	Abductor digiti minimi	2.5-12.5% MVC	Subjects: 8 Repeats: 5
Guzmán et al. (2011)	IZ characterization	Gel-filled cavity	Size: 13x5 IED: 8 mm d : 2 mm	BW: N/S Gain: 2000 f_{amp} : 2048 Hz	Biceps brachii	Voluntary Submaximal	Subjects: 20 Repeats: 3

Chapter 4

Signal analysis

4.1 Introduction

Signal processing is a large part of sEMG. The conventional way of investigating the frequency content of a signal uses Fourier analysis. However, a new method of analysis, with many of the same assumptions, emerged in the early 1980s, called wavelet analysis²⁰. This is based upon the similarity of signal features to wavelets (brief oscillatory waveforms) of different duration. A few years later this was adapted for signal processing by Stephane Mallet. Wavelets offer an elegant alternative to Fourier analysis with some significant advantages as will be discussed in this chapter. Before this, however, I would like to give a brief overview of Fourier analysis in order for a better understanding of Wavelets to be made. Although Fourier and wavelet analysis can be applied to many fields, in relevance to my own research I will be largely discussing these techniques in the application of time-based, 1-dimensional signals.

4.2 Fourier analysis

Joseph Fourier was a 19th century physicist who demonstrated that any periodic function can be written as a linear combination of sine and cosine functions at different frequencies: the Fourier series.

4.2.1 Fourier transforms

The Fourier transform extended Fourier's ideas to represent non-periodic signals in terms of their frequency content. It first translates the function, such as a signal in the time domain,

into a frequency domain function. The Fourier coefficients of the transformed signal represent the contributions of sinusoids at each frequency²⁰. The inverse Fourier transform reverses the process, allowing the conversion from the frequency to the time domain. The Fourier transform, $F(\omega)$, of a function, $f(t)$, and its inverse (together called the Fourier transform pair) are as follows⁶:

$$F(\omega) = \int_{-\infty}^{\infty} f(t)e^{-i\omega t} dt \longleftrightarrow \frac{1}{2\pi} \int_{-\infty}^{\infty} F(\omega)e^{i\omega t} d\omega \quad (4.1)$$

Noticable advances in the field of Fourier analysis include the discrete Fourier transform (DFT), the fast Fourier transform (FFT) and the windowed Fourier transform (WFT) or short time Fourier transform (STFT).

The DFT allows the application of Fourier analysis on a discrete number of sample points (i.e. any digitally sampled signal). It is discrete in time and frequency. The DWT, $X[n]$, of the function of discrete time $x[n]$, where n is an arbitrary sample point, are calculated as follows:

$$X[k] = \sum_{n=0}^{L-1} x[n] e^{-i\frac{2\pi}{N}kn}, \quad k = 0, 1, \dots, N-1 \quad (4.2)$$

4.3 Wavelets

This section introduces the notion of the wavelet, explaining the definitions and parameters. The notion of energy is discussed in the construction of the scalogram.

4.3.1 Basis functions

Wavelets are similar to sinusoids in that they oscillate about the x -axis, integrating to zero. However the oscillations are damped (to zero) thus the function is localized in time or space⁴⁵. Like Fourier analysis, the starting point for wavelet analysis is to represent the signal as a linear combination of a pair of orthogonal basis functions⁶⁰. However wavelet analysis offers a huge advantage over Fourier in that there are many wavelet pairs to choose from, each with different morphologies. The exact pair chosen depends upon a number of factors including: the signal properties, the application and the computational complexity⁴. A wavelet must fulfil the conditions of admissibility and regularity. Mathematically it must meet the following criteria:

1. It must have finite energy

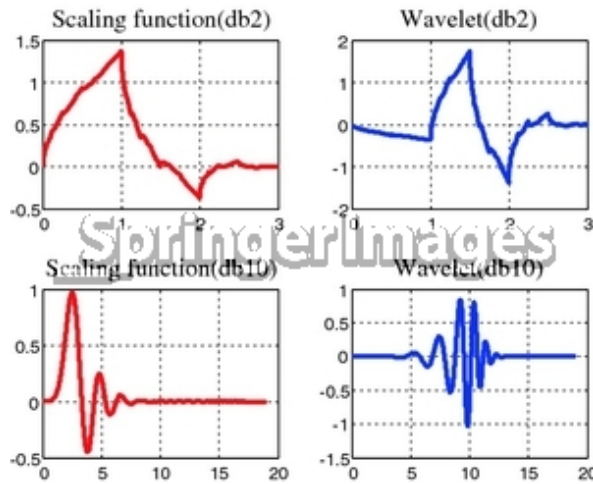


Figure 4.1 – Four different wavelet: (A) the db2 and (B) db5 wavelets, invented by Ingrid Daubechie, and two biorthogonal wavelets, (c) bior1.3 and (d) bior1.5. Image taken from www.SpringerImages.com ©2011

$$E = \int_{-\infty}^{\infty} |\psi(t)|^2 dt < \infty \quad (4.3)$$

2. If $\hat{\psi}(f)$ (is the Fourier transform of $\psi(t)$) then:

$$C_g = \int_0^{\infty} \frac{|\hat{\psi}(t)|^2}{f} df < \infty \quad (4.4)$$

Where C_g is the admissibility constant, which implies $\hat{\psi}(0) = 0$, i.e. it must have no zero-frequency component.

3. Complex wavelets must be real and should vanish for negative frequencies.

Some examples of wavelets are shown in figure 4.1.

The main advantage wavelets have over sinusoids is they are localised in space, whereas sinusoids are considered to be infinitely long⁵⁶. As a consequence, signals transformed into the wavelet domain are much more sparse and so much better at representing discontinuities and sharp spikes in the signal²⁰. For example, a saw-tooth signal sampled at 256 Hz would require 256 sinusoids to represent the discontinuities. However it could be compactly represented by only 16 wavelets⁴ (see figure 4.2). This effective localization with just a few pertinent coefficients makes it particularly useful in signal coding¹.

4.3.2 Dimensions

Rather than transforming signals into their frequency content, wavelet analysis uses a notion called scale. This refers to the size of the wavelet in relation to the signal. Coarse-scale

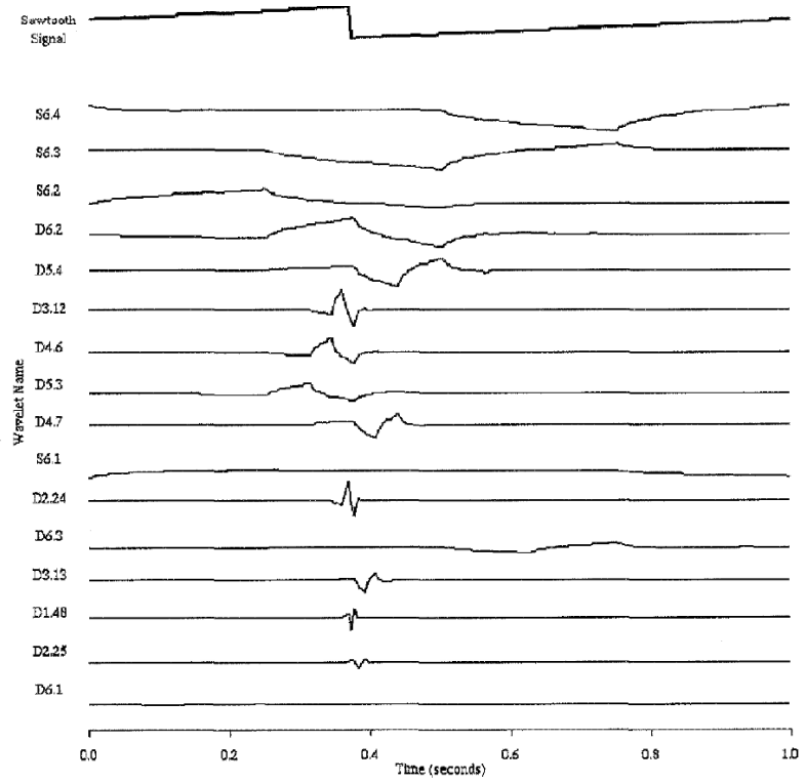


Figure 4.2 – Representation of a sawtooth signal with 16 scaled and time-shifted versions of the db4 wavelet. Image taken from Bruce et al.,⁴ ©1996, IEEE

wavelets cover a large portion and capture the larger trends, fine-scale wavelets are much more localised and capture the sharper details, e.g. see figure 4.2. This suggests that scale is inversely proportional to frequency. In fact the frequency associated with a wavelet of arbitrary scale a is given by:

$$f = \frac{f_c}{a} \quad (4.5)$$

Where f_c is the mother wavelet's characteristic frequency¹. The other dimension used is the location b within the signal. In terms of signal analysis this is analogous to time. The terms a and b will be used to represent arbitrary scales and locations, respectively, in the rest of the chapter.

4.3.3 Energy

Before any wavelet transforms are discussed the concept of (spectral) energy must be introduced. Like the spectrogram of STFT, the signal is characterised by the energy of features at each scale and location, i.e. its energy density surface, or scalogram. Such energy is defined as¹:

$$E(a, b) = |T(a, b)|^2, \quad (4.6)$$

where $T(a, b)$ is the wavelet transform function of a continuous time signal, as discussed in the next section. The scale dependent energy distribution (the relative energy at a specific scale) is given by¹:

$$E(a) = \frac{1}{C_g} \int_{-\infty}^{\infty} |(a, b)i(t)|^2 db \quad (4.7)$$

4.4 Wavelet transforms

The different Fourier transforms are mirrored by analogous wavelet transforms. This section will discuss a few of these, starting with the continuous wavelet transform.

4.4.1 The continuous wavelet transform

The wavelet transform of a continuous signal is defined by the following equation:

$$T_{a,b} = \frac{1}{\sqrt{a}} \int_{-\infty}^{\infty} x(t) \psi^* \left(\frac{t-b}{a} \right) dt \quad (4.8)$$

Where $\psi^*(t)$ is the complex conjugate of the analysing wavelet function $\psi(t)$ and a and b are its dilation and location factors, respectively.

4.4.2 The discrete wavelet transform

The continuous wavelet transform also has a discrete time version. This is derived through power-of-two scaling and dilating in discrete steps⁶⁰. The discretization leads to a wavelet of the form¹:

$$\phi_{m,n} = \frac{1}{\sqrt{a_0^m}} \phi \left(\frac{t - nb_0 a_0^m}{a_0^m} \right) \quad (4.9)$$

Which defines the orthonormal wavelet basis, where $\phi_{m,n}$ is known as the mother or analysing wavelet and m and n are integers controlling wavelet dilation and translation, respectively. The analysing wavelet is used to analyse the data at different resolutions, using the equation:

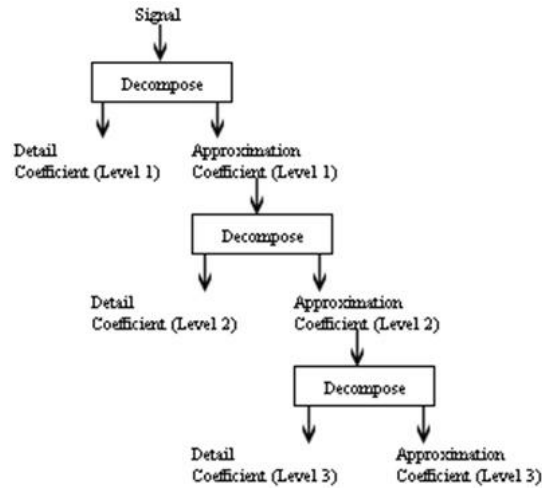


Figure 4.3 – The signal is decomposed through iterations of the scaling wavelet and the analysing wavelet. New details are assumed to contain redundancy due to the preservation of the details from the initial decomposition. Picture from www.originlab.com, ©2011

$$\psi = \sum_{k=-1}^{N-2} (-1)^k c_{k+1} \phi(2x + k) \quad (4.10)$$

Where $\psi(x)$ is the scaling function for the analysing wavelet and c_k are the wavelet coefficients. The wavelet coefficients must satisfy linear and quadratic constraints.

The coefficients $\{c_0, \dots, c_n\}$ act as a filter and are used to produce two transformation matrices²⁰. One (the scaling function, ψ) acts in a similar way to a low-pass filter and serves to smooth the signal to highlight the broad-scale trends. The other (the analysing wavelet) works as a high-pass filter to reveal fine-scale details of the signal. Together they form a quadrature mirror filter pair. The signal is cycled through the quadrature mirror filter pair, splitting its bandwidth in half with each iteration. This is known as multi resolution analysis⁵⁶. Efficient down-sampling operations means that at each iteration, half of the data can be discarded, as shown in figure 4.3.

4.4.3 The wavelet packet transform

The wavelet packet transform (WPT) is a generalization of the DWT that involves the multi-resolution decomposition with a quadrature mirror filter pair¹. However, both approximation and a detail coefficients are kept at each stage. The optimal WPT coefficient is selected to minimize the amount of entropy within the decomposed signal. The most common criterion for selection is the Shannon entropy measure. The decomposition tree structure for the wavelet

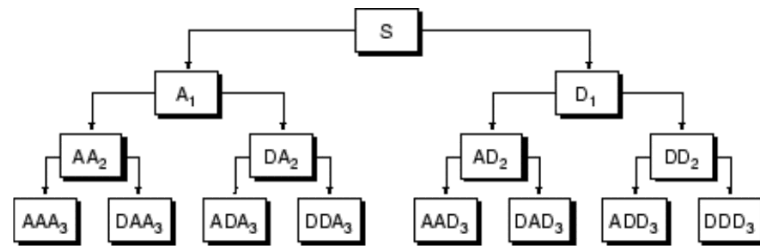


Figure 4.4 – A visual representation of the wavelet packet decomposition process. The raw signal, S , is successively divided into high (details, D) and low (approximations, A) scales, doubling the number of scale bands with each iteration. Picture from www.mathworks.com, ©2011

packet transform is shown in figure 4.4.

4.5 summary

This chapter has briefly discussed some of the techniques applicable to signal processing. Fourier transforms were examined and it was explained how, to some extent, they have been superseded by wavelet analysis. Wavelets are transient, oscillatory signals that can be used as basis functions for the continuous wavelet transform, its discrete time counterpart, and the wavelet packet transform. Although this chapter has not gone into wavelets with any depth, this should provide sufficient information for the experiment to be explained.

Chapter 5

Design considerations

5.1 Introduction

The aim of this section is to explore the parameters and techniques which have to be taken into account in the experimental methods. This includes both the setup and the processing of data. Realistic limitations will have to be taken into account during the design, these include the equipment. The first section explores the acquisition of data, section 2 discusses the signal processing techniques applicable and section 3 considers a suitable method for determining statistical significance from the results.

5.2 Data acquisition

5.2.1 Wrist movement

Currently myoelectrically controlled prosthetic hands usually have two or fewer electrodes, giving only one degree of freedom at most³⁰. Clearly this is unsuitable for recreating the complexity of movement the human hand displays. Furthermore the electrodes usually require activation of physiologically unintuitive muscles, e.g. wrist flexion and extension for hand opening and closing (referred to on as 'hand' grips for the rest of this report).

It is hypothesized that the additional option of being able to open and close the forefinger and thumb (together: 'pinch' grip) individually would be both a significant improvement to the repertoire of the amputee and represent a suitable challenge for the device to distinguish this movement from the anatomically similar hand grip.

5.2.2 Extrinsic hand musculature

Hand and pinch opening, i.e. extension of the finger, or fingers, and thumb both involve many of the same muscles, as do hand and pinch closing. In particular the opening of the fingers is actuated by the extensor digitorum communis and the closing is actuated by the flexor digitorum profundus and superficialis. It is the simultaneous activation of other extrinsic wrist muscles (muscles for hand control located in the wrist) that creates the different overall movement. Unfortunately the flexor digitorum profundus is not a superficial muscle, it is separated from the surface by other muscles (i.e. it is electromyographically occluded), as shown in figure 5.1. The volume conduction effect (as discussed in chapters 2 and 3) dictates that signal quality will deteriorate with depth. The flexor digitorum superficialis is an intermediate layer (with some surface exposure) thus make a more feasible target.

5.2.3 Electrode placement

To characterise the chosen movements, arrays will be placed over the extensor digitorum communis (the superior surface as the arm is rested neutrally with elbow flexion of 90°) and flexor digitorum superficialis (the inferior surface). It will be roughly aligned with the muscle fibres, which run, approximately, diagonally from the tip of the elbow to the thumb. As we are not estimating muscle fibre conduction velocity, or the location of innervation zones the accuracy of alignment is not of particular relevance (see chapter 2 for an explanation). It will be the pattern of activation within the detection volume that is used to distinguish between movements. This requires that the electrodes are in the same positions for each movement.

5.2.4 Array parameters

HD sEMG allows the topographical pattern of activation to be defined with high spatial selectivity. This should allow the movements to be distinguished by much smaller (consistent), spatial differences in muscle (or MU) recruitment. The study is limited to only one size of 2-dimensional array: a 64-channel (13×5) array with interelectrode distance of 8 mm in both directions. This may be insufficient for an estimation of MFCV however it should provide the spatial resolution necessary for gross anatomical features to be identified. This array is self-adhesive with gel-filled, Ag-AgCl lines cavities as electrodes. Both of these are recommended for the removal of movement artefact¹³.

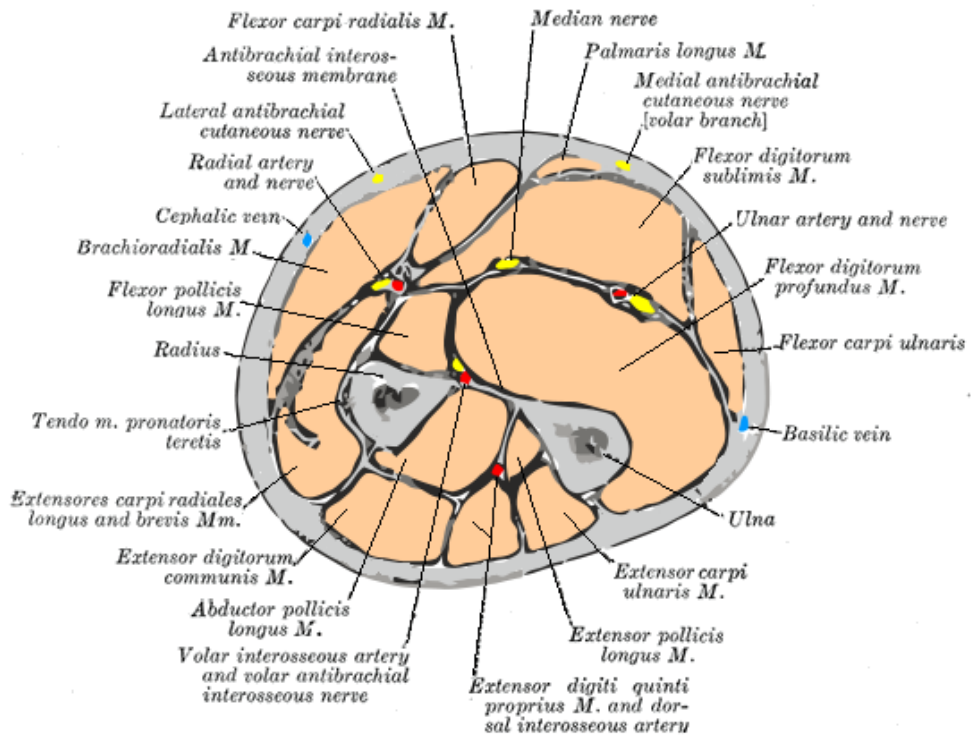


Figure 5.1 – Mid-wrist musculature (cross-section). Picture taken from Wikipedia.org, ©2011.

5.2.5 Recording parameters

The sEMG spectrum has most of its useful information within the 5 to 400 Hz range. A 3dB bandwidth of 10 to 500 Hz proved satisfactory in preliminary testing (results not shown). The Nyquist criterion requires a sampling rate of at least 1000 Hz. In practice a better signal is recorded with much higher frequencies, however more data is needed to represent a given signal length. A 2048 Hz sampling rate was decided upon as a compromise between precision and data size.

5.3 Signal processing

As chapter 3 suggests, HD sEMG requires a great deal of signal processing to be interpreted correctly. Results gained must also be evaluated for significance through statistical analysis. However, the techniques used must be appropriate to the experiment, therefore it is necessary to consider how the muscle can be characterised.

5.3.1 Muscle characterization

Many of the terms and ideas used in this section were discussed in chapter 2, the reader may wish to refer to this chapter where appropriate. Increased neural drive is coupled to a recruitment of greater numbers of MUs (usually with faster firing rates)²³ and an increase in the firing rates of the individual MUs themselves⁷. These properties lend themselves to the characterization of muscular activation through discharge rate. Indeed many decomposition studies rely on the ISI for MUAP identification^{2;10;33;35;36;34}.

Whilst signal amplitude has generally been proposed for multichannel control of prosthetic limbs^{30;43;44;53} there are drawbacks to this approach: MUAP waveforms are unaffected by neural drive⁸, correlation relies on the positive summation between simultaneous MUAPs. However interference is destructive as well as constructive, thus superimposition cannot be relied upon to increase signal amplitude. Various MU properties, such as slight variation in timing, have been shown to effect amplitude cancellation in rectified sEMG³².

5.3.2 Wavelet analysis

The time-frequency properties of the wavelets lend themselves to the analysis of non-stationary signals. It is therefore unsurprising that many sEMG studies have opted for wavelets over more traditional Fourier techniques.

Flanders suggests that the Daubechies family of orthonormal wavelets are particularly well suited to the sEMG due to their morphological similarity to MUAPs¹⁷. The triphasic db2 wavelet (figure 4.1) is the simplest and has been used in various sEMG studies^{28;29}.

There appears to be only a single study applying wavelet analysis to HD sEMG¹⁹ (as discussed in chapter 3). It is suggested that the system (Gazzoni et al.) developed generates a wavelet tailored to individual MUAPs. This would seem to make needless work, thus for this experiment the db2 wavelet has been chosen.

5.3.3 Wavelet transform

The continuous wavelet transform (or its discretised version) is superior to the STFT due its scale-varying window properties where discontinuous, non-stationary signals are to be analysed. However, it was decided in the preceding sections that, given the simplicity of the experiment, recording of the signal initiation and termination would be avoided. The time-frequency properties of the CWT would therefore be redundant.

A recent study by Hu et al.,²⁸ uses the wavelet packet transform to decompose the signal

into discrete scales. The relative energy of the signal at each of these scales was then found, giving the relative wavelet packet energy (RWPE). This was hypothesised as representing the probability of this scale (frequency) being present in the signal and so used as a basis for feature detection. Due to the (relative) simplicity of this technique, and the reported success RWPE will be used to characterise the signal in my experiment. This will be carried out for every channel, offline, using MATLAB 7.10 (The Mathworks, Inc). The various scripts created for this are in Appendix III. In keeping with their design decomposition was carried out to 4 orders, giving 16 scales (as discussed in chapter 4). Lower orders were experimented with in preliminary tests (results not shown) but segmentation of the low scales was insufficient for movement discrimination (i.e. almost the entire signal energy was in just one frequency band).

5.4 Statistical analysis

Statistical analysis gives an estimate of the degree to which we can trust the results. Thus rigorous testing is required before any inferences can be made. Factors to be considered when choosing an appropriate test are discussed in this section.

5.4.1 Variables

The independent variables will be the movement that is performed and the spatial activation pattern. This last factor can be split into the spectral frequency content (which is used as a measure of muscle activation) and the spatial location of the recording site. Thus independent variables are: movement, scale and channel. Note that scale has been discretised through wavelet packet decomposition meaning scale and channel are of interval level data sets only. Movement is categorical as it cannot be ranked. As discussed in the last section these will be quantified though RWPE, at each scale and channel, for every movement, for all individuals.

5.4.2 Method

Due to the large 3-dimensional data sets for each condition, and the number of variables, 3-way analysis of variance will be used to investigate whether variance between movements (over each channel) is statistically greater than variance within each movement. ANOVA has the advantage of being able to investigate the interaction effects between all of the variables, thus an idea of the correlation between them can be inferred.

Each subject used will have a unique physiology in terms of their forearm size, thus it is expected that the arrays will have a different relative spatial density. It is also likely that subjects

will display individual interpretations of the movements. Based on these assumptions it is felt that a comparison between individuals would introduce too many confounding variables, rendering such comparison meaningless. Therefore each individual will have their results analysed individually.

Statistical analysis will be performed with MATLAB 7.10 (The Mathworks, Inc), using the RWPE coefficients generated in the signal processing stage. To help find significance in the results each movement will be repeated 10 times.

A 20 s rest period between repetitions was used to delay the onset of fatigue which could affect the results. Ideally a longer rest would have been preferred, but due to constraints on the subjects' time, a 20 s rest was chosen (thus keeping the entire experiment within a 1 hour limit without reducing the number of repeats). Fatigue has been shown to affect MU firing properties. To compensate for the effects of fatigue each subject will carry out their sequence of movements in a different order.

5.5 Summary

In this section factors important to the design of the experiment were discussed. These factors included the movements to be chosen, the recording parameters, signal processing and statistical analysis. The actual method used will be discussed in the following chapter.

Chapter 6

Methods

Information regarding the methods during the experiment are discussed in this chapter. The decision on these design parameters were explored in the previous chapter. In the first section acquisition of the HD sEMG is explained, in terms of the materials used and the recording procedure. The techniques used to process and analyse the raw data are explained in the subsequent section.

6.1 HD sEMG Acquisition

6.1.1 Subjects

Five healthy volunteers (age 24-30, one male and four females), without signs of muscular disorder, gave their informed consent to participate in this study.

6.1.2 Equipment

The myoelectric signal was recorded with two high-density, flexible electrode arrays. Each array consisted of 64 electrodes (Ag-AgCl-lined cavities) arranged in a 5 (columns) by 13 (rows) matrix, with one corner electrode missing (OT Bioelettronica, Torino, Italy), as shown in figure 6.1. The interelectrode distance was 8 mm and the electrode diameter was 2 mm. The electrode cavities were filled with an electro-conductive paste (ac-cream, Spes Medica s.r.l., Battipaglia, Italy). Each array was connected with four electrically shielded, 16-channel cables (AD1x16SD5, OT Bioelettronica, Torino, Italy). Cables were kept as separate as possible but due to the confined space contact between them was unavoidable, this was most noticeable at the electrode attachment ports. The 128 channels were amplified using a single-differential

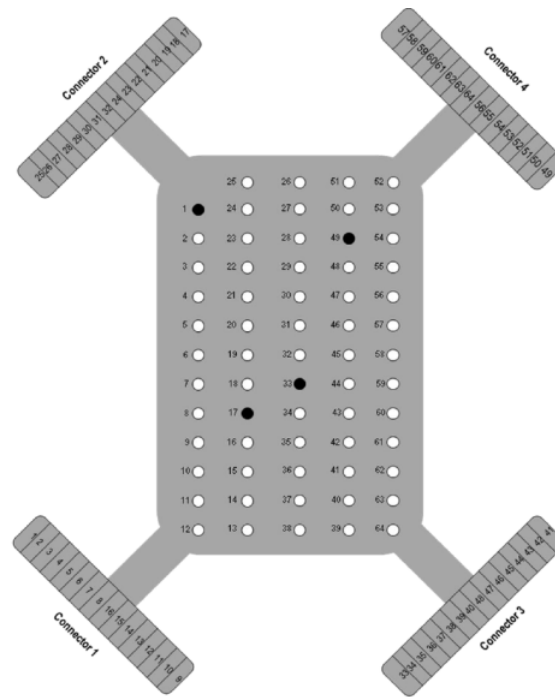


Figure 6.1 – The layout of the 64-channel HD array used for sEMG recording. The black channels indicate the split between output ports. Note that columns run antiparallel to each other. Array (ELSCH064R3S) and diagram supplied by OT Bioelettronica, Torino, Italy, ©2011

configuration, whereby each channel had the signal from the channel immediately below it in the column subtracted from it, with a 256-channel purpose-built amplifier (USB-EMG2, OT Bioelettronica, Torino, Italy) resulting in 118 bipolar channels. Note that columns ran antiparallel to each other as shown in figure 6.1. A hard-wired bandpass filter applied a 3db bandwidth of 10-500 Hz. The gain was set to 1000 and the analogue-digital conversion was performed at a sampling frequency of 2048 Hz at 12 bits of resolution. The signal was recorded using custom-designed software for the amplifier (OT Biolab, OT Bioelettronics, Torino, Italy).

6.1.3 Setup

The area was initially prepared with a dermo-abrasive paste (everi, Spes Medica s.r.l., Battipaglia, Italy) to remove dead skin, a high source of impedance, and cleaned with alcohol to remove any grease.

The arrays were mounted on double-sided adhesive foam pads which served to fix them to the skin. The first array was then affixed over the muscle belly of the right flexor digitorum superficialis and the second was affixed over the extensor digitorum communis. The columns were aligned roughly parallel with the muscle fibres. Medipore tape (3M, Berkshire, UK) was used for extra security and to prevent electrode-paste from escaping through electrode openings



Figure 6.2 – Two foam covered blocks were used as armrests. The base of each was made from wood and two metal rods maintained a fixed difference. The rods had various holes in the ends so that the separation of the blocks could be adjusted for physiological variation in arm length.



Figure 6.3 – A thermosetting acrylic sheet was cut and moulded around a hollow cylinder. A slit allowed the finger tips to slide underneath a section, thus isometric extension and flexion of the fingers was possible. A cord looped through the cylinder and provided isometric resistance against thumb extension. During the experiment the device was mounted to a rod in the desk (not shown).

and shorting the channels.

6.1.4 Protocol

The right arm was rest on two contoured custom-built foam blocks, one at the wrist and one at the elbow (see figure 6.2). These negated the need for muscular support yet kept the electrodes free of external pressures. It also made cable management easier.

Each subject used a custom-built manipulandum which allowed isometric resistance against the movements which would be used (see figure 6.3).

Four movements were chosen for testing: opening and closing the entire hand ('hand grip') and opening and closing just the index-finger and thumb ('pinch grip'). These were explained to the subjects in advance, through verbal and visual demonstration and instructions are included with the consent form.

Each movement was held for 5 s and repeated 10 times by all subjects. A 20 s rest period between repetitions was used to delay the onset of fatigue which could affect the results. A one minute rest period separated each set of movements in which the subjects were reminded of the next movement. Each subject carried out their movements in a different order to randomize the effects of fatigue. At the very start and end of the experiment, and between every different movement set, each subject performed a 20 s negative control. During this the arm was kept as relaxed as possible whilst the sEMG signal was recorded. The subjects were asked to perform the movement at (roughly) between 30-50% of their maximum possible contraction.

6.2 Data analysis

Data analysis was carried out offline using Matlab 7.10 (The Mathworks,) and consists of three parts: Signal conversion, wavelet packet analysis and statistical analysis. Signal conversion and wavelet packet analysis were merged into a single script (See Appendix III: GETSIG.M). Statistical analysis consisted of two separate scripts: one to display descriptive statistics (Appendix III: WPSTD.M) and the other to test for significance (Appendix III: WPANOVAN.M).

6.2.1 Signal conversion

This step was necessary to extract the data from the binary signal file and reorganise the data to compensate for the antiparallel arrangement of channels. Channels that were corrupted by interference were removed. The last channel from each column, which gave a meaningless signal due to bipolar derivation (which results in one fewer leads per column) was also removed. Note that to maintain consistency between conditions, corrupt channels were removed from all results. The removal of inferior-quality channels is common to many HD sEMG designs (e.g. see Chapter 3). This stage also had a function to display the remaining channels as a single graph (in the correct order). This was repeated for every signal.

6.2.2 Wavelet Packet analysis

Once the signal had been reordered, wavelet packet decomposition was applied to each channel iteratively. Decomposition was to the 4th order, dividing each signal into 16 compartments according to scale (scale bins). Entropy type used was Steins unbiased risk estimator (SURE) as it takes into account signal length, with the formula:

$$SURE = \sqrt{2 \log(s_i \log_2(s_i))} \quad (6.1)$$

Where SURE is the threshold for entropy and s_i is the signal length. The relative energy at each scale (for every channel) was then found. This was repeated for every signal.

6.2.3 Statistical analysis

The first script takes the output from wavelet packet analysis and calculates the mean energy values (for every channel at every scale) for the repeats of a single movement, by a single individual. This was repeated for each movement type (including the controls) of each individual. The standard deviation was also taken along with each mean value, using the adjusted formula.

The second script applied 3-way analysis of variance (ANOVA) on the results to see if variance between different movements was significantly greater than variance within the same movement. This was done on an individual-by-individual basis, as variation in individual physiology and experimental setup would have introduced too many confounding variables for a statistical comparison across individuals. The factors investigated for effect and interaction were scale, channel and movement type. Significant rearrangement of the data was necessary to create the (indexed) column vector format that MATLAB required.

Chapter 7

Results

In this chapter the relative wavelet packet energy (RWPE) distributions are illustrated for the movements made by each individual. Due to the amount of data generated (10 repeats \times 5 movements \times 5 subjects = 250 conditions) only the means and standard deviations for each repeat are shown. The full data is available on request to those that are interested.

Unfortunately there seemed to be problems with the signals from the array placed over the flexor digitorum superficialis (the 'flexor' array). They were of very low amplitude yet the raw signal showed some anatomical features, including similarity of signal between channels aligned with the muscle fibre and an inversion of the signal around a point suggesting the location of the motor end plates. Thus it was felt that the signal was valid. However, after starting with 118 bipolar channels (59 for each array) a total of 15 channels had to be removed due to significant corruption through artefact, leaving 103 channels. All of which were from the flexor array. Wavelet packet decomposition was to the 4th order, thus there were 16 scale bands. This meant each repeat is represented by 103x16 matrix of RWPE coefficients, which was used to form a surface plot. This was a significant reduction in data size from the raw signal which was approximately 103x10230 (samples). Channels 1-59 are taken from the array on the upper surface of the arm (extensor array, which covered the extensor digitorum communis) and channels 60-103 are from the flexor array. Based on these observations it was decided not to reject the channels from this array, which accounts for the 15 omitted channels. The cause of this drop in signal volume is unknown, however this array required an extra adaptor to be plugged into the amplifier that was not needed for the other array.

The experiment aims to find discriminant features within each movement, allowing it to be distinguished from other movement by its spatial distribution RWPE features. Thus, this chapter will be split into those space-frequency features that are common to more than one movement (section 2) and those that are observed in just a single movement (section 3), helping to identify

spatial or temporal features that may be applicable to pattern recognition. A complete statistical analysis of the results was unavailable due to computational limitations, however several movements (within individual) have been compared using 3-way ANOVA and reference to their significance will be mentioned where appropriate. Such analysis is always between either hand and pinch flexion movements or between hand and pinch extension movements. The descriptive data is collated in the next section to avoid breaking up the text.

7.1 Graphs

This section contains the RWPE surface plots for each individual. Movement type is displayed above each individual plot. The control conditions are displayed first so that a judgment of baseline noise and unintentional MUAP firings can be made through visual inspection. A table of results for the 3-way ANOVA carried out between select movements for individuals is also included (table 7.1).

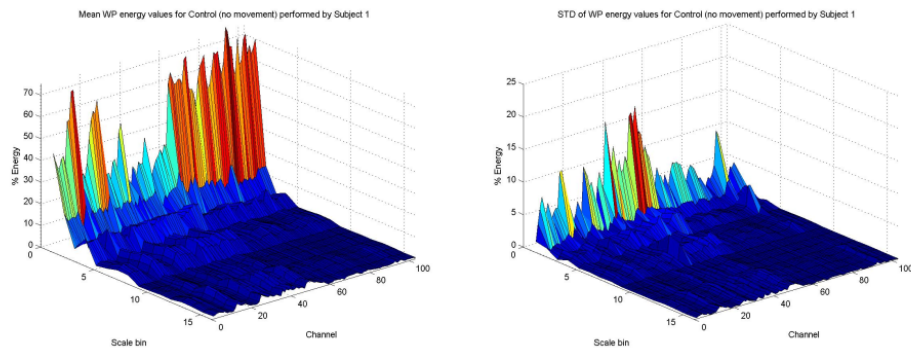


Figure 7.1 – Mean values and standard deviations for the (negative) control condition for Subject 1. Controls were taken between each movement set, thus are representative of the entire experimental duration

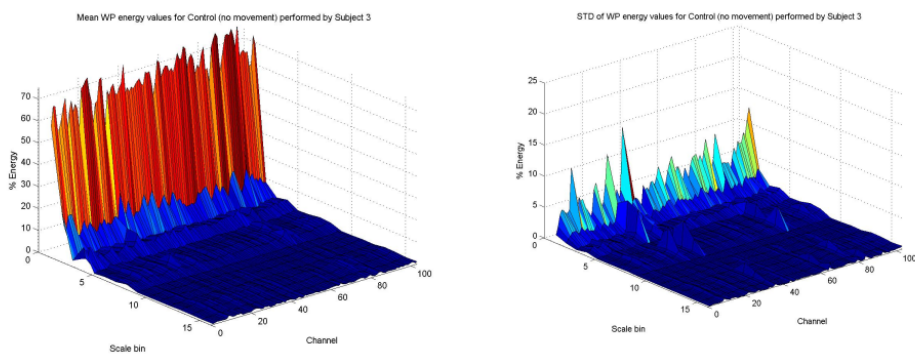


Figure 7.2 – Mean values and standard deviations for the (negative) control condition for Subject 2. Controls were taken between each movement set, thus are representative of the entire experimental duration

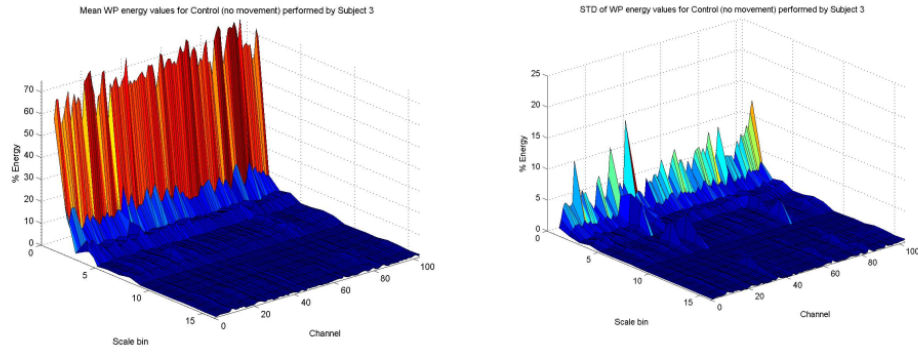


Figure 7.3 – Mean values and standard deviations for the (negative) control condition for Subject 3. Controls were taken between each movement set, thus are representative of the entire experimental duration

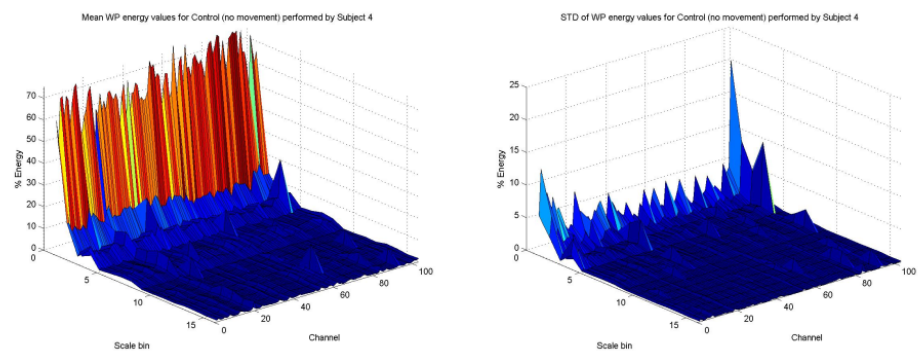


Figure 7.4 – Mean values and standard deviations for the (negative) control condition shown for Subject 4. Controls were taken between each movement set, thus are representative of the entire experimental duration

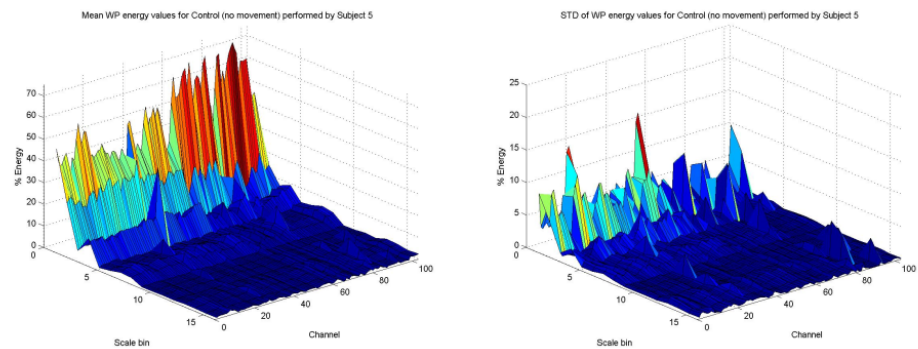


Figure 7.5 – Mean values and standard deviations for the (negative) control condition shown for Subject 5. Controls were taken between each movement set, thus are representative of the entire experimental duration

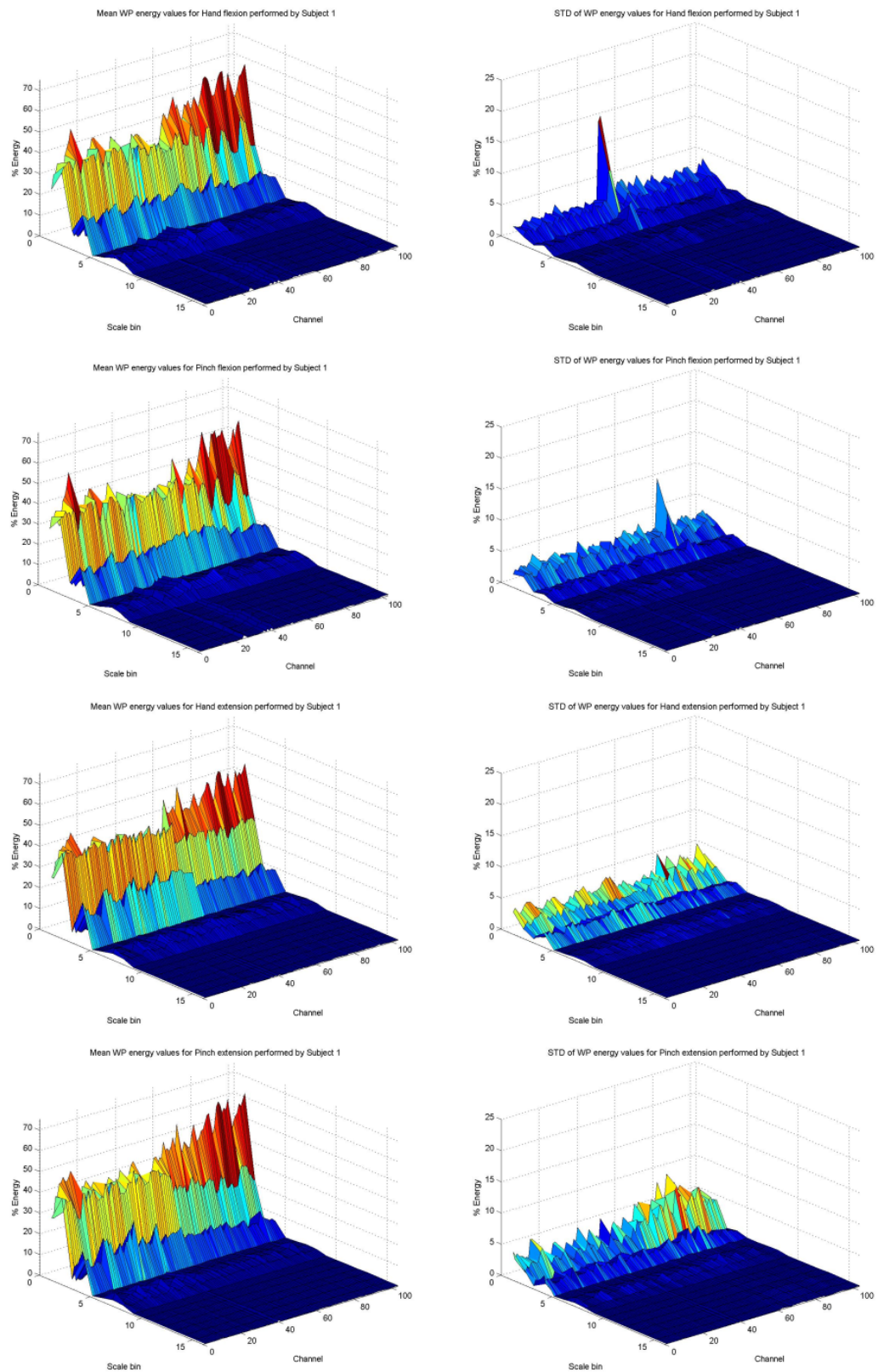


Figure 7.6 – The RWPE coefficients for subject 1. Mean values and standard deviations for the (negative) control condition shown. Controls were taken between each movement set, thus are representative of the entire experimental duration.

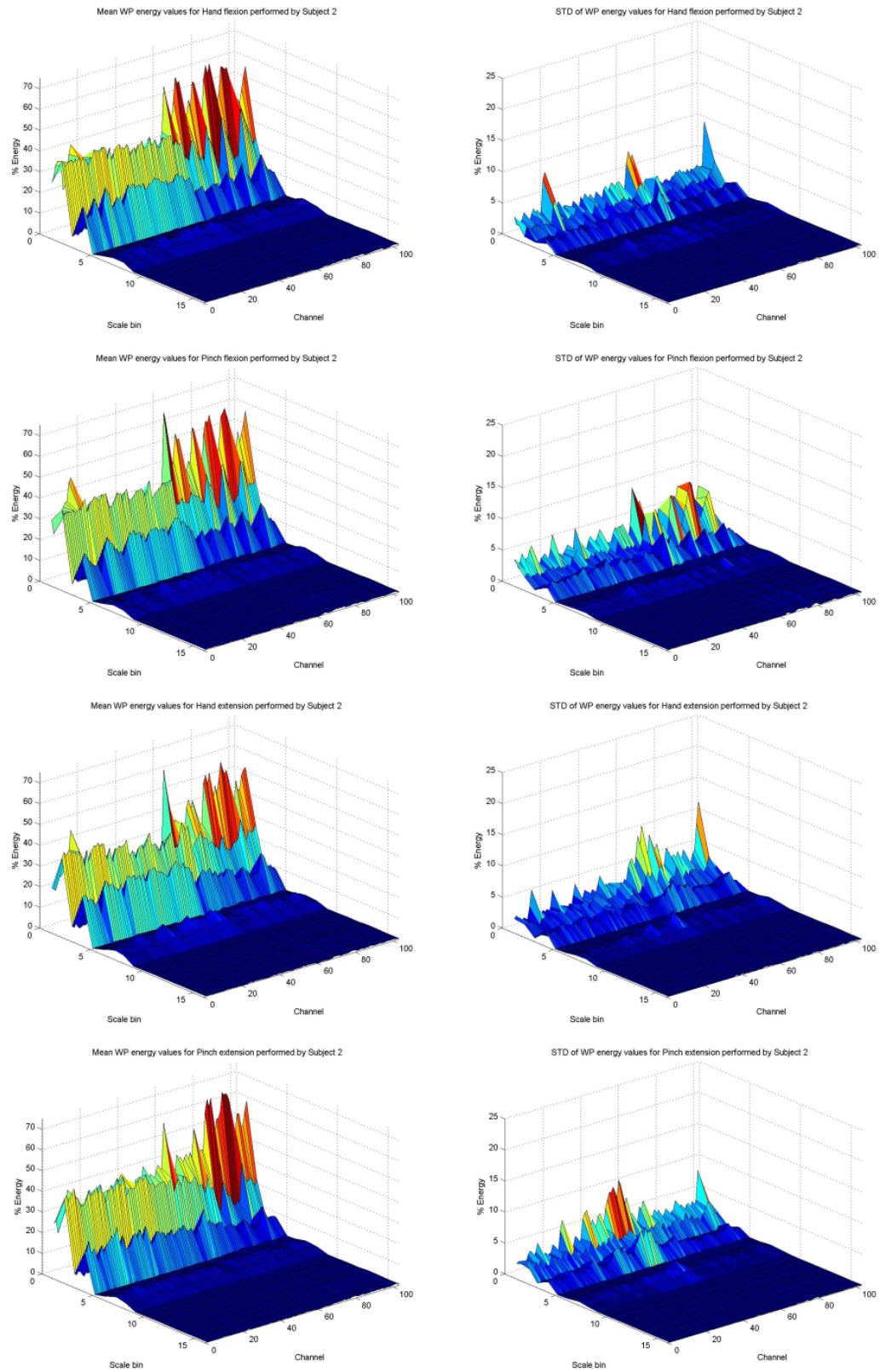


Figure 7.7 – The RWPE coefficients for subject 2. Mean values and standard deviations for the (negative) control condition shown. Controls were taken between each movement set, thus are representative of the entire experimental duration.

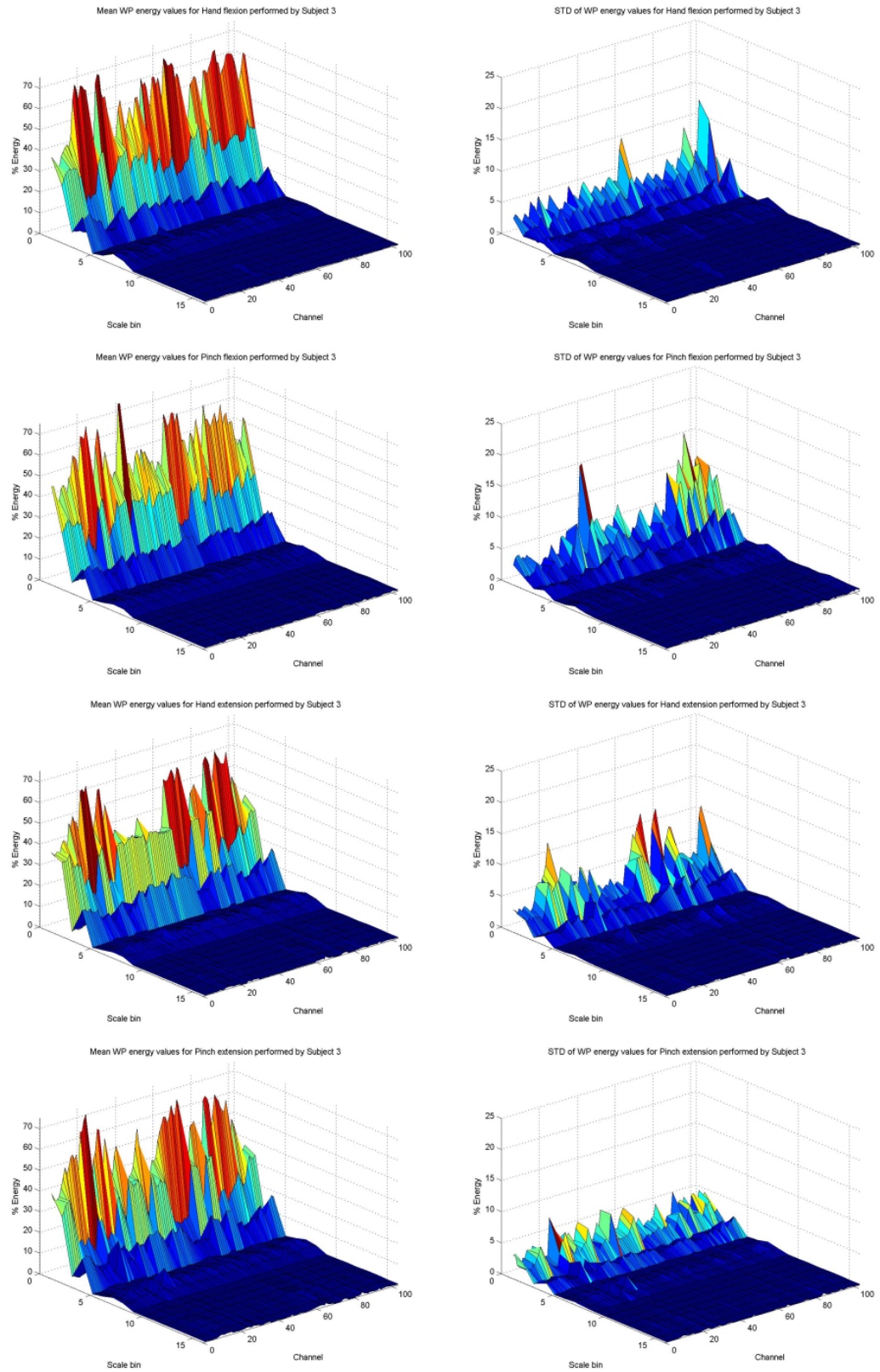


Figure 7.8 – The RWPE coefficients for subject 3. Mean values and standard deviations for the (negative) control condition shown. Controls were taken between each movement set, thus are representative of the entire experimental duration.

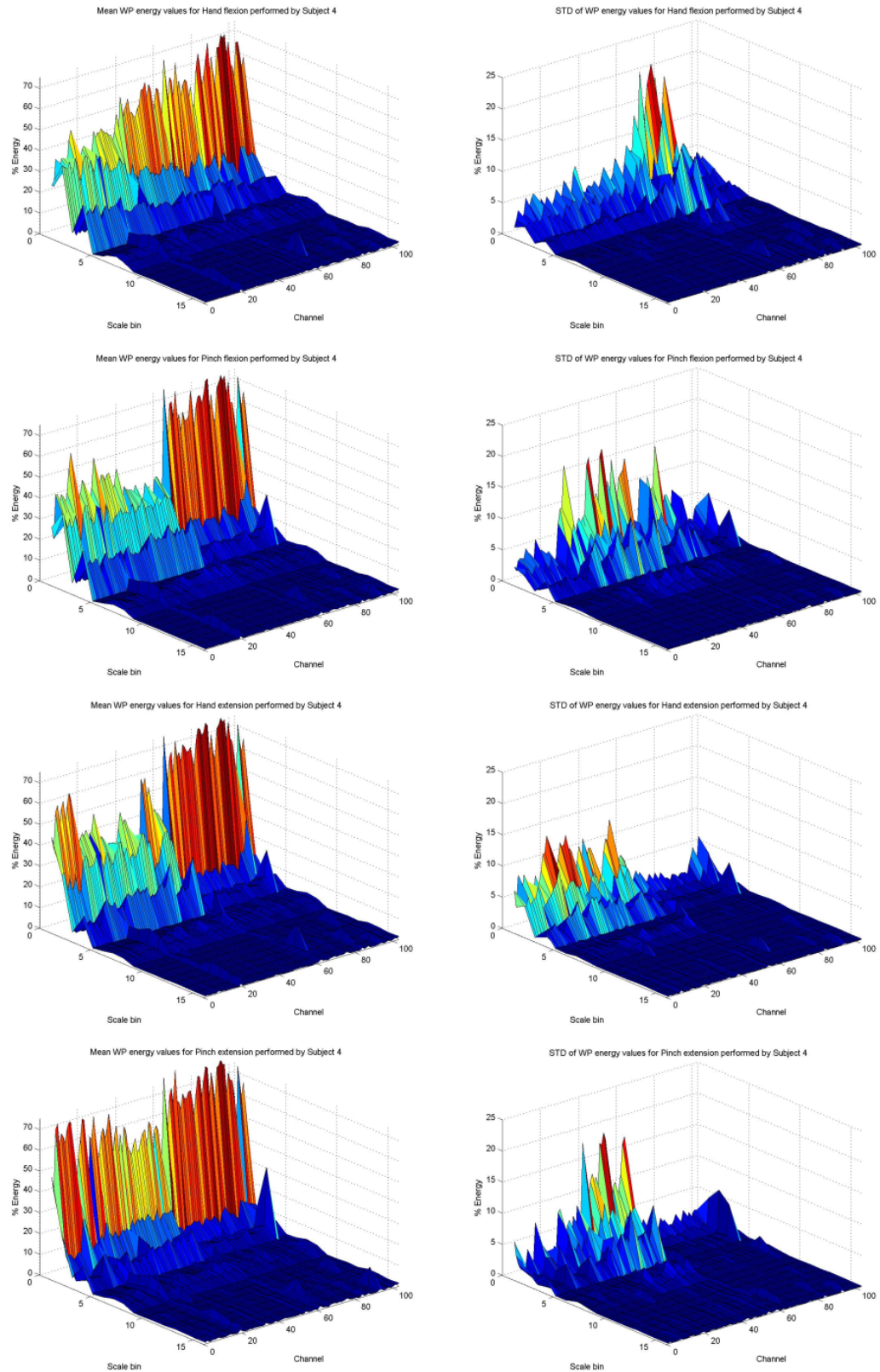


Figure 7.9 – The RWPE coefficients for subject 4. Mean values and standard deviations for the (negative) control condition shown. Controls were taken between each movement set, thus are representative of the entire experimental duration.

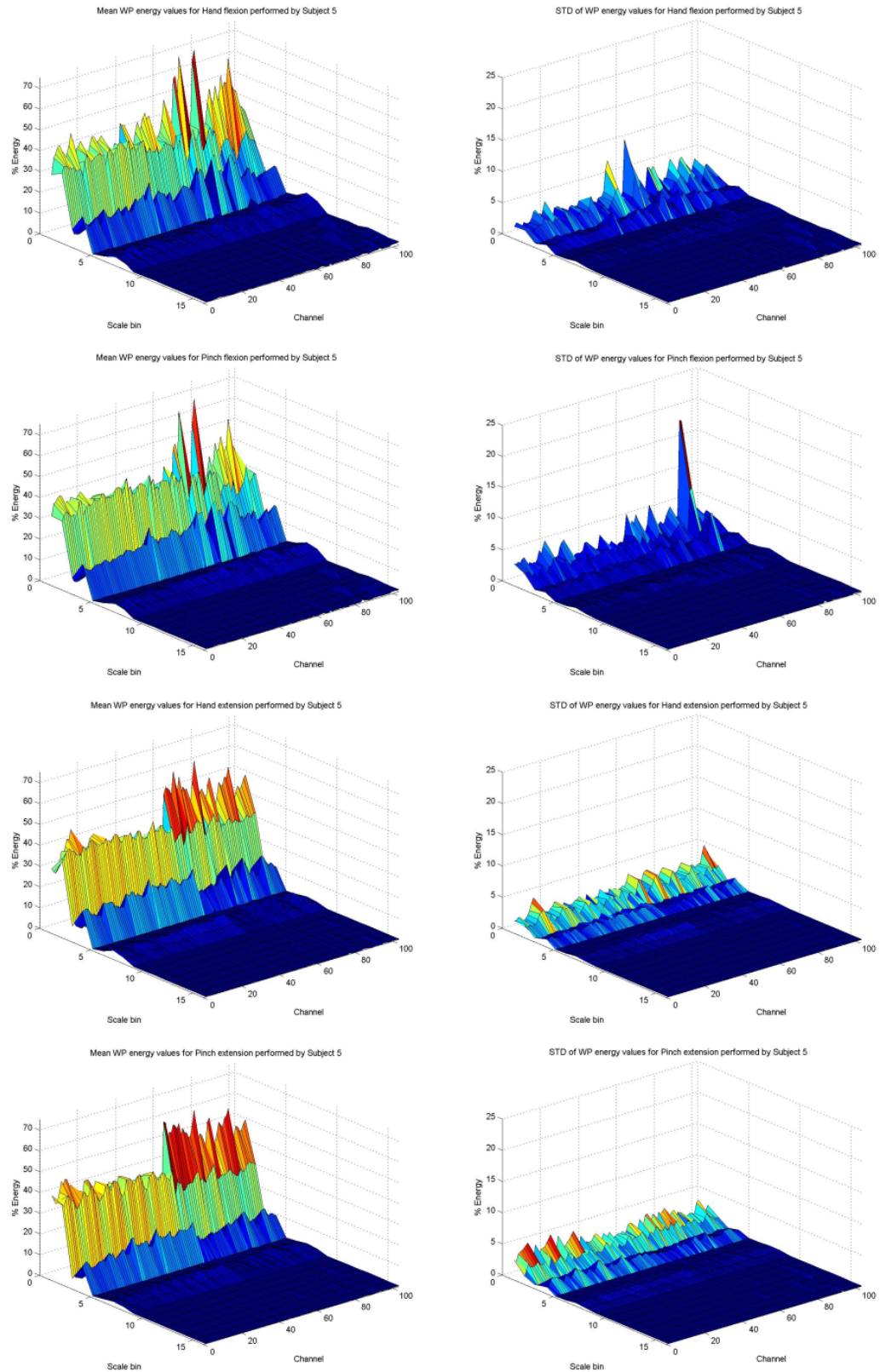


Figure 7.10 – The RWPE coefficients for subject 5. Mean values and standard deviations for the (negative) control condition shown. Controls were taken between each movement set, thus are representative of the entire experimental duration.

H]

Table 7.1 – Results of a 3-way ANOVA between selected conditions

Subject	Movement 1	Movement 2	Interaction (F)	$p > F$
1	Hand close	Pinch close	0.86	~ 1
2	Hand close	Pinch close	0.61	~ 1
3	Hand close	Pinch close	1.85	~ 0
3	Hand open	Pinch open	0.84	~ 1
4	Hand close	Pinch close	1.34	~ 0
4	Hand open	Pinch open	1.17	~ 0
5	Hand close	Pinch close	1.02	0.2584

7.2 Common features

The results in the preceding section show the mean values of the wavelet packet energy density surface, respectively, and also the standard deviation for each mean. It should be pointed out the RWPE is only the ratio of frequencies within a single channel. Inferences between the relative amount of muscle activation cannot be made through direct comparison with other channels. However, higher frequencies can indicate an increased neural drive. The movements all share some common features:

1. Along the frequency axis a pattern of three local maxima emerges, with peaks at scales 7, 4 and 2 or 1. This is seen in all movements and to some extent in the control, occurring in the means and in the standard deviation plots. The first scale-peak seems to be fairly similar between movements. The second one seems to show more variation and may be a better marker for pattern recognition (as discussed in the next chapter).
2. The dominant energies are mostly in the detail coefficients, at scale 1, which corresponds to the higher frequencies. This is most obvious at the higher channels, which correspond to the flexor array.
3. The majority of movements also show some scale 1-peaks in the low channels (1-20) in many of the movements, although such peaks are generally lower in this (extensor) array than in the flexor array. The range of RWPE coefficients in scale 1 is similar in each flexor (roughly 30-60%) however it tends to be between 40-50% in the flexor array and around 30% in the extensor array. The standard deviation at this scale band is generally less than 4% of the total energy, which is roughly about 10-15% of the energy at this scale. However considerable variance in standard deviation is seen between individuals and movements for some channels.
4. The movement conditions seem to be much more similar to each other than to the control condition, where no movement was made. The high energies in scales 1 (highest frequencies) suggest that this band may contain a great deal of noise.

7.3 Discriminant features

This section will systematically discuss some of the features that distinguish particular movements from each other. This will be done separately for each subject as inferences between subjects are confounded by unavoidable extraneous variables (as discussed in chapter 5).

7.3.1 Subject 1

In the control condition (figure 7.1) there is more energy, in the high scales, in the flexor matrix than the extensor. Similarly the range is larger at these scales, with this matrix, as shown by the standard deviation. There appears to be nothing obvious by which to differentiate movements within subject 1 (figure 7.6). The results of a 3-way ANOVA between hand and pinch flexion (table 7.1 suggest that the interaction between the three variables is not significant ($p \approx 1$), i.e. no significant inferences can be drawn from the relationship between the three factors, suggesting that this setup would be unsuitable for a means of distinguishing the movement.

The hand and pinch flexion movement each show one channel with a relatively huge standard deviation, several times larger than the other channels, suggesting a much larger spread of data. The standard deviations seem to be higher in the flexor array for extension movements than flexion movements, possibly suggesting that more variation in muscle activation is seen when the extensors are the antagonistic muscles.

7.3.2 Subject 2

As with subject 1, figure 7.7 shows that the lowest scale dominates the signal in all subject recordings, but especially in the flexor array. The responses from hand and pinch extension movements appear very similar. This similarity is much more noticeable in the inferior array (channels above 59). This pattern is also seen in the responses from hand and pinch flexion. ANOVA showed that interactions between variables were not significant between hand and pinch flexion movements ($p \approx 1$).

7.3.3 Subject 3

Figure 7.8 shows several of the peaks seen in the hand flexion movement to be reduced in magnitude during pinch flexion. ANOVA showed significant interaction between all factors ($p \approx 0$) for these movements suggesting that (for this individual) differentiation based upon the spatial distribution of RWPE coefficients may be possible. Although there appeared to be some variation in RWPE coefficients between extension movements, ANOVA (table 7.1) was

unable to find significant interactions ($p \approx 1$).

7.3.4 Subject 4

Different patterns of energy distribution are observed at scales 1 and 4 for the hand and pinch flexion movements from the extensor array, as shown in figure 7.9. The flexor array seemed to be largely dominated by the lowest scale, for all movements however. Despite this, significant interactions were found between the hand and pinch flexion ($p \approx 0$) and also between hand and pinch extension ($p \approx 0$) using ANOVA (table 7.1). This strongly suggests that it may be possible to find discriminant features capable of classifying these moves, for this individual.

7.3.5 Subject 5

The distribution of RWPE coefficients was very similar between flexion movements and between extension movements (figure 7.9), although standard deviations showed that the range of RWPE coefficients was quite small (figure 7.9). ANOVA (table 7.1) revealed that interactions between the flexion movements was not significant ($p = 0.2584$).

Chapter 8

Discussion

This chapter will evaluate the results found in the last chapter. Section 1 will discuss the principle findings and what can be inferred from these. Section 2 will examine alternative methods of prosthetic control using HD sEMG (of which there is currently little published work). Section 3 will discuss some of the limitations of the experiment, and how they relate to the principle findings identified in section 1. Section 4 will suggest some ways in which the experiment could be improved for future studies.

8.1 Principle findings

The aim of this experiment was to see if hand movements could be characterised by the distribution of MUAP firing frequency patterns as recorded by HD sEMG. The similarity shown between spectral distributions in the previous chapter, along with the rather limited statistical analysis at present, suggest that the current experimental setup used would be largely unreliable as a means of characterising hand movements. Further statistical analysis was unfortunately prevented due to computational complexity of carrying out 3-way ANOVA on such a large data set. Thus we must presume, at present anyway, that this subset of results is indicative of the entire data set. Some significant interactions were found between certain movements, scales and channels, e.g. subject 4, implying that it may be possible to extract specific discriminant features using these methods. However development of the technique would be necessary for the characterization of hand movements using HD sEMG and RWPE to be viable. Some suggestions as to how the reliability of the technique could be improved will be discussed later in this chapter.

The idea of using RWPE for the spectral analysis was taken from Hu et al.²⁹ who used the

technique to decompose a bipolar signal into distinguishable forearm actions. Rather more success was reported than in this study, however. This may be due to the additional feature extraction algorithm that was applied to the data to generate (what they called) RWPE features. RWPE features were based on characteristic patterns within the signal, equivalent to the peaks seen within channels in my results. However these features were averaged across subjects and then merged if a correlation seemed likely (to compensate for its lack in a particular individual). Due to the imprecise nature of the electrode placement in my experiment, and changes in anatomy between individuals (which would alter the distribution of tissue beneath the array) this option was not possible, therefore many repeats were taken to compensate for this. Despite this the results have only presented occasional significance.

It may be possible to increase the significance of interactions between movement, scale and channel by reducing the number of channels and/or the scales chosen. The fact that almost all of the signal energy was at scale 1 (the highest frequency band) during the negative control strongly suggests that this frequency was largely noise. The removal of this could help determine a pattern in the remaining frequency bands. Similarly some channels may be better than others at representing the underlying muscular activity involved in different movements. As we are measuring gross anatomical features, rather than individual motor units, the inclusion of so many channels may contain a great deal of redundant information. In particular the high scales (9-16), which contained a very small proportion of the signal energy (if any) may have had a blanketing effect on the ANOVA tests. I.e. the variance at these scales will be very low for each channel and for each movement. Indeed, examination of the ANOVA tables (shown in Appendix II) showed that variance between channels was not significant.

Pruning the selection down to a pertinent few may help achieve significant interaction between the three terms. It would be fairly easy (although possibly not very quick) to rewrite the MATLAB scripts to use a reduced number of scales (possibly only one or two would be needed) and/or channels. The reduced complexity of the 3-way ANOVA may also make statistical testing more feasible (in terms of computational demands). However there are inherent dangers in searching for significance using post hoc-analysis, altering the experimental parameters to suit the results. A way around this could be to try and repeat the experiment using the new parameters, should significance be made available. One further problem with reducing the number of channels is that either an algorithm would have to be created to select the most pertinent channels or a subjective estimate would have to be made. The former would represent a considerable challenge, whereas the second generates problems with reproducibility and precludes the use to those without sufficient anatomical knowledge. These were the two (successful) options used by Huang et al. to increase the efficacy of prosthetic control through targeted muscle reinnervation³⁰ as was discussed in chapter 3.

8.2 Alternative research

The literature is very sparse on the subject of using HD sEMG for optimising prosthetic control. I was only able to find two studies using a fixed-distance, multidimensional electrode array both by Nagata et al.^{43,44}, although they were both summaries of proceedings from conferences, rather than journal articles. The first of these used only one column of 16 electrodes (out of the 96 channel grid) to increase the response time. Channels were selected through pretesting, using all 96 channels, and then a canonical discriminant analysis was used to identify the EMG patterns as the principle eigenvectors of the data. The second study also used canonical discriminant analysis but the pretesting stage calculated the most pertinent channels for accurate classification. Both of these techniques used signal amplitude, rather than firing rate, which can cause problems when trying to infer neural drive (as discussed in chapters 2 and 5) as it relies on spatial summation of different MUs rather than temporal summation within individual MUs.

The other two studies relied on single channel electrodes arranged over the surface in a two-dimensional array. The study by Huang et al.³⁰, which was mentioned in the previous section, has already been discussed in detail in chapter 3. The remaining study, by Tenore et al. is another summary of proceedings from a conference⁵³. This used principle component analysis to characterise the movements by several time-domain features: amplitude, wavelength, absolute mean and variance. An artificial neural network was used to for pattern recognition.

In terms of studies combining wavelet analysis with HD sEMG, only one was found. This was by Gazoni et al.¹⁹ who used the continuous wavelet transform (see chapter 4) to extract MUAPs from the sEMG interference signal. In this case the use of wavelets was described as a limiting factor since it was not possible to represent the changes to an arbitrary MUAP waveform with spatial distribution accurately with the wavelet basis function.

8.3 Limitations

As discussed in the results chapter, the experiment was limited by the multi-adaptor needed for connection of the second (flexor) matrix. It is possible that the signal was damped within this or the gain was somehow compromised using the multi-adaptor input port of the amplifier. Testing of this equipment has not yet been carried out to determine the cause of this problem.

The data collated in the results section suggests that noise is the overriding feature of the signal. Noise is generally of a higher frequency than the EMG spectra⁵² and the lowest scale (the highest frequency band) tended to dominate the RWPE surface plots. This is especially prevalent in the control conditions. The wavelet packet transform acts as a bank of quadrature mirror filters²⁰

(see chapter 4), breaking up the signal into separate scale bands. Thus it has innate abilities to (roughly) filter out specific unwanted frequencies. As discussed in previous sections this limiting factor could quite easily be removed through the omission of the lowest scale. Normalisation would have to be made so the summation of the remaining RWPE coefficients equalled 100% of the total signal energy.

Another method to reduce noise could be to try a different function for entropy selection during wavelet decomposition. In this experiment SURE (Stein's unbiased risk estimator) was used as a criterion for setting the threshold of 'unwanted' signal components. Altering the entropy thresholding function may remove noise, which is generally considered to have high entropy¹².

8.4 Future work

This experiment was based around characterising the spatial distribution of motor unit activation using their frequency content (i.e. firing rate) which is linked to neural drive⁸ (see chapter 2). As discussed in earlier sections of this chapter, neural drive to the motor system is displayed by temporal recruitment (an increase in MU firing rate) and spatial recruitment¹⁴). As each MU tends to fire at a different frequency²³ (to prevent synchronous firing) both of these aspects are frequency dependent. However, it may not be difficult to incorporate a function to compare maps of the topographical muscular activation, based on signal amplitude. This could either aid in the selection of useful channels for characterization by frequency, or could add another dimension to the analysis. This last idea must be approached cautiously, however, as adding a new continuous variable to the already overburdened ANOVA computation would be unlikely to be successful without a significant removal of data from elsewhere.

8.5 Conclusion

This chapter discussed the results that were gained from the experiment and suggestions as to how to overcome some of the limitations that were identified. Comparisons to other work was carried out and some studies of HD electromyographic prosthetic control were mentioned. Several relatively simple improvements to the analysis of results were suggested, however, due to time constraints the efficacy of these cannot be tested.

Chapter 9

Summary and Conclusion

9.1 Introduction

This final chapter attempts to summarise this report. The previous chapters are summarised in the first section and the experiment is evaluated, with respect to the aim, in the latter.

9.2 Summary of chapters

Chapter 2 began with a brief overview of the anatomy of muscle, with emphasis on motor units and their action potentials. This was necessary for an understanding of sEMG which was explored in the succeeding sections, culminating in a description of HD sEMG. Several important concepts were also introduced, including superimposition, spatial filtering and spatial sampling. These concepts were explored further in chapter 3, which comprised a literature review of papers concerning HD sEMG. The majority of papers reviewed were concerned with decomposition, i.e. deconstructing the surface signal into component MUAPs. A distinction was made between decomposition procedures requiring user-interaction and those that incorporated fully-automatic algorithms.

Chapter 4 began with a brief discussion on Fourier analysis, the traditional methods for signal processing. This led onto wavelet analysis, a more recent invention, which has several advantages over Fourier. Most noticeably these include the ability to examine the signal at different scales simultaneously and at different time locations. Continuous and discrete time wavelet transforms were discussed along with the wavelet packet transform.

The concepts discussed in the previous chapters were used to justify the experimental methods in chapter 5. The precise methodology was then outlined in chapter 6.

Chapter 7 contains the experimental results. Each hand movement (from each subject) was condensed to show just the means and standard deviations of RWPE coefficients for every channel and scale. ANOVA results were also shown for interaction effects between (within-subject) experimental variables for several movement combinations. Unfortunately a comprehensive analysis was impossible due to computational (and time) limitations.

The significance of the results was discussed in chapter 8. Some results showed significant (within-subject) variance between movements whilst others did not. There were no similar studies for comparison but several studies which contained relevant elements were mentioned. Limitations of the experiments (and analysis) were posited and several avenues for further study, including possible methods of increasing significance, were suggested.

9.3 Evaluation

The aim of this project was to investigate whether hand movements could be characterised by the activation pattern seen in the extrinsic hand musculature (in the wrist) using HD sEMG. It was theorised that firing frequency would represent muscle activation more reliably than firing magnitude. Thus WP analysis was applied to the acquisition of spectral frequency information at each (spatially distinct) channel.

Whilst several of the results suggested that such analysis could enable an accurate discrimination of hand movement, a lack of consistency means that the method is probably too unreliable without alteration. As discussed in chapter 8, however, several key changes to the analysis may give substantial improvements to the reliability (i.e. the significance). Therefore, despite the mixed success of this experiment, this research definitely does not appear to constitute a dead end.

Appendices

Appendix I: Glossary of terms

ANN - See **Artificial neural network**.

ANOVA - See **Analysis of variance**

Artificial neural network - A computer model that is based on biological neural systems. Through weighted connections it is able to adapt to new information.

Blind-identification - See **Blind-source separation**.

blind-source separation - A method for MUAP extraction where no assumptions are made about the underlying MUAP physiology other than each MU displays statistical independence (e.g. see Holobar et al., 2004).

CKC - See **Convolution kernel compensation**.

continuous wavelet transform - A real-time time-frequency analysis technique whereby (1 or 2D) signals are characterised by scale (frequency) and location (time or distance).

convolution kernel compensation - A blind-source separation technique using the products of convolutions to represent MUAPs (e.g. see Holobar et al., 2007).

HD - See **High-density**

HD sEMG - See **High-density surface electromyography**.

high density array - A 2-dimensional array of densely spaced electrodes, of fixed interelectrode distance, for use in sEMG.

high-density surface electromyography - sEMG performed with a high density array.

ICA - See **Independent component analysis**.

ICT - See **Incremental counting technique**.

IED - See **Inter-electrode distance**.

iEMG - See **Intramuscular electromyography**.

In silico - Performed on a computer or by computer simulation.

Incremental counting technique - A method for MUNE involving the successive activation of MUs through artificially evoked responses.

Independent component analysis - Statistical technique using eigenvectors to reduce dimensionality of datasets whilst maintaining the most important (variance) features.

Innervation zone - The point at which the motoneuron synapses with the muscle fibre. See also neuromuscular junction.

Inter-electrode distance - The distance by which the (centres) of two electrodes are separated.

Inter-spike interval - A method of classifying MUAPs by the timing delay between consecutive firings.

Intramuscular electromyography - An (invasive) means of recording electrical activity in the muscle through the insertion of a needle.

ISI - See **Interspike interval**.

IZ - See **Innervation zone**.

Lead - The theoretical channel that may be the output of several a spatial filter.

Linear time invariant - A system is linear time invariant if the relationship between input and output is linear and unaffected by a time delay.

LTI - See **Linear time invariant**.

MART ANN - See **Multichannel adaptive resonance theory ANN**.

MFCV - See **Muscle fibre conduction velocity**.

Motor unit - The functional unit of the muscle.

Motor unit action potential - The sudden, transient change in voltage across the muscle fibre membrane accompanying signal propagation.

Motor unit number estimation - A method of estimating the total MU population within a detection volume, also see **Incremental counting technique**.

MPS - See **Multiple-point stimulation**.

MU - See **Motor unit**.

MUAP - See **Motor unit action potential**.

Multichannel adaptive resonance theory ANN - Consists of a set of ART2 neural networks (one per channel in parallel to compare patterns between channels and output similarity. Applied to MUAP decomposition by Gazzoni et al. (2004).

MUNE - See **Motor unit number estimation**

Muscle fibre conduction velocity - The propagation velocity of the electrochemical impulse along the muscle fibre (usually averaged over entire fibre length unless otherwise specified).

Neuromuscular junction - The synapse of the motor neuron on the muscle.

Nyquist - The Nyquist criterion states a signal must be sampled at a minimum of twice the highest frequency in its bandwidth to avoid low frequency artifacts (the Nyquist limit).

Rectified sEMG - An sEMG signal that has had negative amplitudes reversed in polarity.

Scalogram - A means of depicting the relationship between time and frequency for a signal using wavelet analysis.

sEMG - See **Surface electromyography**.

Spatial filter - The weighted sum of a specific configurations of two or more electrodes, resulting in a high-pass filtering effect in the spatial domain.

Steins unbiased risk estimator - A method for assigning criteria for the rejection of scales during wavelet packet decomposition based upon the entropy at that scale.

SURE - See **Steins unbiased risk estimator**.

Surface electromyography - A technique for measuring neuromuscular potentials from the surface of the body.

Targeted muscle reinnervation - A technique to reroute motor neurons to redundant muscles following amputation (e.g. see Zhou et al., 2005).

TES - See **Transcutaneous electric stimulation**.

TMS - See **Transcranial magnetic stimulation**.

Transcranial magnetic stimulation - The evocation of a muscular response through magnetically activating parts of the motor cortex.

Transcutaneous electric stimulation - The evocation of a muscular response through electrical stimulation across the skin.

Underdetermined system - If there are N sources from M linear mixes and $M < N$ then the underlying system is underdetermined, i.e. it has multiple solutions.

Wards clustering - Hierarchical clustering method based upon Euclidean distances (e.g. Klein et al., 2007).

Wavelet - A brief oscillatory waveform used as a basis function for wavelet analysis.

Wavelet packet transform - A function for sequentially dividing a signal by scale using wavelets as high and low-pass filters.

WPT - See **Wavelet packet transform**.

Appendix II: ANOVA tables

Table 1 – Results of 3-way ANOVA for Subject 1 for interactions between hand and pinch flexion.

Analysis of Variance					
Source	Sum Sq.	d. f.	Mean Sq.	F	Prob>F
Scale	4264658	15	284310.5	30819.19	0
Channel	0	102	0	0	1
Movement	1	1	1	0.11	0.742
Scale*Channel*Movement	12117	1530	7.9	0.86	1
Error	288847.5	31311	9.2		
Total	4565621	32959			

Table 2 – Results of 3-way ANOVA for Subject 2 for interactions between hand and pinch flexion.

Analysis of Variance					
Source	Sum Sq.	d. f.	Mean Sq.	F	Prob>F
Scale	3823944.5	15	254929.6	14560.81	0
Channel	0.5	102	0	0	1
Movement	0.5	1	0.5	0.03	0.8658
Scale*Channel*Movement	16351.8	1530	10.7	0.61	1
Error	548190.8	31311	17.5		
Total	4388486	32959			

Table 3 – Results of 3-way ANOVA for Subject 3 for interactions between hand and pinch flexion.

Analysis of Variance					
Source	Sum Sq.	d. f.	Mean Sq.	F	Prob>F
Scale	5824536.5	15	388302.4	32557.57	0
Channel	0	102	0	0	1
Movement	6	1	6	0.5	0.4782
Scale*Channel*Movement	33774	1530	22.1	1.85	0
Error	373435	31311	11.9		
Total	6231746	32959			

Table 4 – Results of 3-way ANOVA for Subject 3 for interactions between hand and pinch extension.

Analysis of Variance					
Source	Sum Sq.	d. f.	Mean Sq.	F	Prob>F
Scale	4805332	15	320355.5	18184.15	0
Channel	0	102	0	0	1
Movement	-3.5	1	-3.5	-0.2	0
Scale*Channel*Movement	22738	1530	14.9	0.84	1
Error	551615	31311	17.6		
Total	5379684.5	32959			

Table 5 – Results of 3-way ANOVA for Subject 4 for interactions between hand and pinch flexion.

Analysis of Variance					
Source	Sum Sq.	d. f.	Mean Sq.	F	Prob>F
Scale	5116142.5	15	341076.2	14121.41	0
Channel	-1	102	-0	-0	0
Movement	1.5	1	1.5	0.06	0.8032
Scale*Channel*Movement	49474.5	1530	32.3	1.34	0
Error	756258.5	31311	24.2		
Total	5921876.5	32959			

Table 6 – Results of 3-way ANOVA for Subject 4 for interactions between hand and pinch extension.

Analysis of Variance					
Source	Sum Sq.	d. f.	Mean Sq.	F	Prob>F
Scale	6367389	15	424492.6	16889.68	0
Channel	0	102	0	0	1
Movement	-1.5	1	-1.5	-0.06	0
Scale*Channel*Movement	44829	1530	29.3	1.17	0
Error	786947.5	31311	25.1		
Total	7199167	32959			

Table 7 – Results of 3-way ANOVA for Subject 5 for interactions between hand and pinch flexion.

Analysis of Variance					
Source	Sum Sq.	d. f.	Mean Sq.	F	Prob>F
Scale	4079144.8	15	271943	25045.28	0
Channel	0.5	102	0	0	1
Movement	-0.5	1	-0.5	-0.05	0
Scale*Channel*Movement	17008	1530	11.1	1.02	0.2584
Error	339976.5	31311	10.9		
Total	4436129.5	32959			

Appendix III: MATLAB code

This appendix displays the MATLAB scripts used in the analysis of data.

GETSIG.M

This script extracts and reorganise the raw data and to calculate the RWPE for each channel. Several options are built in, including different orders of wavelet packet decomposition.

```
1  % A script to for the command 'GETSIG.M'
2  % Extracts EMG signal features acquired using EMG-USB2
3  % Also analyzes spectral energy using wavelet packets
4  % Written by Thomas Harrison with thanks to OTBioelettronica
5
6  while 2==2           % Conditional program loop
7  close all           % Close all figures
8  clear all           % Clear all variables
9
10     %% DATA ACQUISITION
11
12  % EXPERIMENTAL PARAMETERS -----
13
14  % Ask if default values of samp freq and gain are wanted
15
16  questr = 'Would you like to use default values (samp freq = 2048Hz, gain = 1000)?'
17  yesno = questdlg(questr, 'Sampling parameters', 'Yes', 'No', 'Yes');
18  switch yesno
19      case 'Yes'
20          fsamp = 2048;           % Default sampling frequency
21          Gain = 1000;           % Default gain
22
23      case 'No'
24          fsamp=input('Enter sampling frequency: '); % Input sample frequency ...
25          % in Hz
26          Gain=input('Enter gain: '); % Input gain
27
28  end
29  Offset_plot = 1;           % Offset to separate plotted channels
30  Acquired.Ch = 128;         % Number of acquired channels
31  Plotted.Ch = 128;         % Number of channels that will be plotted
32
33  % Ask the user to choose a signal file
34  [file_name, file_path] = uigetfile('*.sig','Select the Signal file');
35  filename = [file_path file_name];
36
37  % SIGNAL INPUT -----
38  hh=fopen(filename,'r');    % Open file
39  Raw_sig = [];             % Matrix conditioning
40  Raw_sig = fread(hh,[Acquired.Ch, inf],'short'); % Extract bin file
41  fclose all;
42
43  clear hh filename
44
45  % SIGNAL CONVERSION -----
46  Sig = [];                 % Matrix conditioning
47  Sig = Raw_sig*5/2^12/Gain*1000; % Estimates the amplitude on the skin:
48  % 5 is the A/D input range in V
49  % 2^12 take into account the resolution of the A/D
50  % Gain: provide the amplitude on the skin
```

```

51                                     % 1000: convert the amplitude in mV
52 clear Raw_sig
53
54 [nch Sig_dur] = size(Sig);           % Extract Matrix dimensions
55
56 t = linspace(1, Sig_dur/fsamp, Sig_dur); % Time vector in s
57
58
59 %% COLUMN CORRECTION
60 % To realign columns;
61 % correcting for HD-grid zig-zag positioning
62 % and removing last channel in each column
63
64 % COLUMN SPLITTING -----
65 % Last channel in each column is not extracted as bipolar derivation
66 % Alternate columns are flipped to align channels in spatial order
67
68 % Superior array
69 Sig1 = Sig(01:11,:);                 % Extract column 1
70 Sig2 = Sig(13:24,:);                 % Extract column 2
71 Sig2 = flipud(Sig2);                 % Flip column 2
72 Sig3 = Sig(26:37,:);                 % Extract column 3
73 Sig4 = Sig(39:50,:);                 % Extract column 4
74 Sig4 = flipud(Sig4);                 % Flip column 4
75 Sig5 = Sig(52:63,:);                 % Extract column 5
76
77 % Inferior forearm
78 Sig6 = Sig(65:75,:);                 % Extract column 1
79 Sig6 = Sig6([2 4 5 6 7 8 9 10 11],:); % Remove corrupted channels
80 Sig7 = Sig(77:88,:);                 % Extract column 2
81 Sig7 = Sig7([1 2 3 5 6 7 8 9],:);    % Remove corrupted channels
82 Sig7 = flipud(Sig7);                 % Flip column 2
83 Sig8 = Sig(90:101,:);                 % Extract column 3
84 Sig8 = Sig8([1 4 5 6 8 9 10 11],:); % Remove corrupted channels
85 Sig9 = Sig(103:114,:);                 % Extract column 4
86 Sig9 = Sig9([1 2 3 4 5 8 9 10 11 12],:); % Remove corrupted channels
87 Sig9 = flipud(Sig9);                 % Flip column 4
88 Sig10 = Sig(116:127,:);                 % Extract column 5
89 Sig10 = Sig10([1 2 3 4 7 8 9 10 11],:); % Remove corrupted channels
90
91 % COLUMN MERGING -----
92 sig = zeros(103, Sig_dur);           % Create empty matrix
93 sig(01:11,:) = Sig1;                  % Insert column1
94 sig(12:23,:) = Sig2;                  % Insert column2
95 sig(24:35,:) = Sig3;                  % Insert column3
96 sig(36:47,:) = Sig4;                  % Insert column4
97 sig(48:59,:) = Sig5;                  % Insert column5
98
99 sig(60:68,:) = Sig6;                  % Insert column1 array2
100 sig(69:76,:) = Sig7;                  % Insert column2 array2
101 sig(77:84,:) = Sig8;                  % Insert column3 array2
102 sig(85:94,:) = Sig9;                  % Insert column3 array2
103 sig(95:103,:) = Sig10;                 % Insert column4 array2
104
105 clear Sig1 Sig2 Sig3 Sig4 Sig5 Sig6 Sig7 Sig8 Sig9 Sig10
106
107 %% WAVELET PACKET ANALYSIS
108
109 quest2 = 'Which wavelet packet decomposition order is required?';
110 wpcord = questdlg(quest2, 'Decomposition order', '2nd', '3rd', '4th', '4th');
111
112 switch wpcord
113     case '2nd'
114         wpcord = 2;
115         enmat = zeros(64,4);           % Create blank matrix
116
117     case '3rd'
118         wpcord = 3;
119         enmat = zeros(64,8);           % Create blank matrix
120

```

```

121     case '4th'
122         wpdord = 4;
123         enmat = zeros(64,16); % Create blank matrix
124     end
125
126     % Calculate the SURE threshold 'suren'
127     suren = sqrt(2.*log(Sig_dur.*log2(Sig_dur)));
128
129     % WP decomposition of Data matrix
130     % using db2 wavelet to decomp level 4 with SURE entropy
131     for i=1:103;
132         tmpsig = sig(i,:);
133         %suren = thselect(tmpsig,'rigrsure'); % Automatic SURE thr gen
134         T = wpdec(tmpsig,wpdord,'db2','sure',suren); % WP decomposition
135         E = wenergy(T); % Energy of packets
136         enmat(i,:) = E; % Insert energy coeffs
137         clear E T tmpsig % Remove unnec. variables
138     end
139 end
140
141 %% FURTHER PROCESSING
142
143 plotname = genvarname(file_name); % Create string variable name from file name
144
145 plotname = plotname(1:7); % Shorten string to 9 characters
146
147 questr = ['Save details as ' plotname '?'];
148
149 namebutton = questdlg(questr, 'Name?', 'yes', 'no', 'yes');
150
151 switch namebutton
152     case 'yes'
153         % Keep automatic string name
154     case 'no'
155         plotname = input('Save figure and coefficients as? ','s');
156         % Enter new name
157 end
158
159 save(plotname, 'enmat'); % Save energy matrix (current ...
    dir)
160
161 %% GRAPHICAL OUTPUT
162 % Surface plot of wp energy coefficients -----
163
164 surf(enmat); % Surface plot
165
166 h = gcf; % Assign figure handle
167
168 % Graph headings
169 title(['Surface plot of wavelet packet energy coefficients (' plotname ')']);
170 xlabel('Scale bin'); ylabel('Channel'); zlabel('% Energy');
171
172 % Set graph axes (16 x 103 x 75)
173 axis([0 16 0 103 0 75]);
174
175 saveas(h,plotname,'fig'); % Save figure (current dir)
176
177 %subplot(1,2,1), surf(enmat); % Place in subplot
178 %title('Surface plot of wavelet packet energy coefficients');
179 %xlabel('Scale bin'); ylabel('Channel'); zlabel('Energy');
180 %
181 % Channel-by-channel visualization -----
182 %
183 %for i = 1:103 % Plot the desired channels
184 % subplot(1,2,2), plot(t, sig(i,:)+Offset_plot*(i));
185 % hold on
186 %end
187 %
188 %hold off
189

```

```
190 %
191 % Plot graph of data
192 %title('EMG Data (all channels)');
193 %xlabel('Time (s)');
194 %ylabel('Signal amplitude (mV)');
195
196
197 %% REPEAT LOOP
198
199 % Ask if another iteration is required
200 K=menu('Would you like to process more data?','yes','no');
201 if K==1
202     continue
203 end
204 if K==2
205     disp('Thanks for using this program')
206     break
207 end
208
209 delete K
210
211 end
```

COMPSTD.M

This script compares movements performed by each individual, using data generated with the previous GETSIG.M script. It takes the mean values and standard deviations for each set of repeats. Several menus are provided for accurate labeling of figures.

```

1  %% COMPSTD.M
2  % A script to compare 10 WPE matrices from the same movement
3  % All from the same individual
4  % Outputs will be 2 graphs:
5  %     - mean value for each node
6  %     - standard deviation for each node
7  % % N.B. WPE = wavelet packet energy
8  % Matrix enmat created with GETSIG.M
9  %
10 % Created by Thomas Harrison, 14/08/2011
11
12
13 %% Movement Classification
14
15 % Menu for movement classification
16 menuquestrg = 'Please pick the movement category from the options below';
17 menop1 = 'Hand flexion';
18 menop2 = 'Hand extension';
19 menop3 = 'Pinch flexion';
20 menop4 = 'Pinch extension';
21 menop5 = 'Control (no movement)';
22
23
24 %Menu to acquire movement type
25 movtyp = menu(['Movement 1:' menuquestrg],menop1,menop2,menop3,menop4,menop5);
26
27 if movtyp == 1
28     mov = menop1;
29 elseif movtyp == 2
30     mov = menop2;
31 elseif movtyp == 3
32     mov = menop3;
33 elseif movtyp == 4
34     mov = menop4;
35 elseif movtyp == 5
36     mov = menop5;
37 end
38
39 %% Subject classification
40
41 menuquestrg = 'Who was the subject?';           % Menu question string
42 menop1 = 'Radhika';
43 menop2 = 'Sibani';
44 menop3 = 'Claire';
45 menop4 = 'Mayank';
46 menop5 = 'Monica';
47
48 % Menu for choosing subject name
49 % Note actual name will not be displayed for confidentiality
50 subjnam = menu(menuquestrg,menop1,menop2,menop3,menop4,menop5);
51
52 % Give anonymous identifiers to subjects
53 if subjnam == 1
54     subj = 'Subject 1';
55 elseif subjnam == 2
56     subj = 'Subject 2';
57 elseif subjnam == 3
58     subj = 'Subject 3';
59 elseif subjnam == 4
60     subj = 'Subject 4';
61 elseif subjnam == 5
62     subj = 'Subject 5';

```

```

63 end
64
65 %% Load files
66
67 qstring = ['Please load the 10 ' mov ' files from the same individual'];
68 button = questdlg(qstring, 'Load movement', 'Ok', 'Ok');
69 switch button
70     case 'Ok'
71
72         uiopen('LOAD');           % Open 1st file of movement
73         mov1 = enmat;
74
75         uiopen('LOAD');           % Open 2nd file of movement
76         mov2 = enmat;
77
78         uiopen('LOAD');           % Open 3rd file of movement
79         mov3 = enmat;
80
81         uiopen('LOAD');           % Open 4th file of movement
82         mov4 = enmat;
83
84         uiopen('LOAD');           % Open 5th file of movement
85         mov5 = enmat;
86
87         uiopen('LOAD');           % Open 6th file of movement
88         mov6 = enmat;
89
90         uiopen('LOAD');           % Open 7th file of movement
91         mov7 = enmat;
92
93         uiopen('LOAD');           % Open 8th file of movement
94         mov8 = enmat;
95
96         uiopen('LOAD');           % Open 9th file of movement
97         mov9 = enmat;
98
99         uiopen('LOAD');           % Open 10th file of movement
100        mov0 = enmat;
101
102    end
103
104 %% Name generation
105 % Automatically create a relevant name string based on subject and movements
106
107 name1 = genvarname(mov);           % Create string variable name
108 name1 = name1([1 6:7]);           % Shorten name1
109 name2 = genvarname(subj);         % Create string variable name
110 name2 = name2([1:4 8]);           % Shorten name2
111 name = [name2 '_' name1];         % Concatenate name
112 clear name1 name2
113
114 questr = ['Save figure as ' name '?'];
115
116 namebutton = questdlg(questr, 'Name?', 'yes', 'no', 'yes');
117 switch namebutton
118     case 'yes'
119                                     % Keep automatic string name
120     case 'no'
121         name = input('Save figure as? ', 's'); % Enter new name
122
123 end
124
125 %% 3D array
126 % Concatenate matrices into a 3-dimensional array
127 movcat = cat(3, mov1, mov2, mov3, mov4, mov5, mov6, mov7, mov8, mov9, mov0);
128 clear mov1 mov2 mov3 mov4 mov5 mov6 mov7 mov8 mov9 mov0
129
130 %% Discriptive data
131 % Creates and saves plots of data parameters
132

```

```
133
134     % Create matrix of mean values
135     meancat = mean(movcat,3);
136     name1 = [name '_mean'];           % Append name with function
137     save(name1, 'meancat');          % Save energy matrix (current dir)
138
139     % Create matrix of STD
140     % Note: this is sample adjusted (N-1)
141     stdcat = std(movcat,0,3);
142     name2 = [name '_std'];           % Append name with function
143     save(name2, 'stdcat');          % Save energy matrix (current dir)
144
145     % Plot matrix of mean values
146     surf(meancat); axis([0 16 0 103 0 75]); view([50,30]);
147     title(['Mean WP energy values for ' mov ' performed by ' subj]);
148     xlabel('Scale bin'); ylabel('Channel'); zlabel('% Energy');
149     fig1 = gcf;                      % Assign figure handle
150     saveas(fig1,name1,'fig');        % Save figure 1 (current dir)
151     saveas(fig1,name1,'jpg');        % Save figure 1 as .jpeg
152
153     % Plot matrix of standard deviations
154     surf(stdcat); axis([0 16 0 103 0 25]); view([50,30]);
155     title(['STD of WP energy values for ' mov ' performed by ' subj]);
156     xlabel('Scale bin'); ylabel('Channel'); zlabel('% Energy');
157     fig2 = gcf;                      % Assign figure handle
158     saveas(fig2,name2,'fig');        % Save figure 2 (current dir)
159     saveas(fig2,name2,'jpg');        % Save figure 2 as .jpeg
160
161 close all
```

WPANOVAN.M

This script loads up the data generated from GETSIG.M and arranges it in a way that MATLAB can interpret for 3-way ANOVA. ANOVA is then carried out. Options allow different numbers of moves to be compared (within the same individual).

```

1  %% WPANOVA.M
2  % A script to do the following:
3      % extract wp energy data from .mat files
4      % convert wp matrix into column vector
5      % place coefficients in the correct order, as follows:
6          % Column 1 = wp energy value (from enmat) = Variable 1
7          % Column 2 = scale bin = Variable 2
8          % Column 3 = channel = Variable 3
9          % Column 4 = hand movement = Variable 4
10         % [See diagram below for example]
11     % Run N-Way ANOVA on new matrix
12
13 % Diagram of column input:
14 % Energy Scale Channel Move
15 % [val] 1-16 1-128 1-5
16 % ... ..
17
18
19 %% Movement ...?
20
21 % Menu for number of input movements (variable 1)
22 questrg = 'How many movements would you like to compare?';
23 nomov = menu(questrg,'5','4','3','2');
24     if nomov == 1
25         nomov = 5;
26     elseif nomov == 2
27         nomov = 4;
28     elseif nomov == 3
29         nomov = 3;
30     elseif nomov ==4
31         nomov = 2
32     end
33
34 % Menu for movement classification
35 menuquestrg = 'Please pick the movement category from the options below';
36 menop1 = 'Hand Flexion';
37 menop2 = 'Hand Extension';
38 menop3 = 'Pinch Flexion';
39 menop4 = 'Pinch Extension';
40 menop5 = 'Control (no movement)';
41
42 for m=1:nomov
43     if m==1 % Generate name string for figures
44         movltyp = menu(['Movement 1:' ...
45             menuquestrg],menop1,menop2,menop3,menop4,menop5);
46
47         if movltyp == 1
48             mov1 = menop1;
49         elseif movltyp == 2
50             mov1 = menop2;
51         elseif movltyp == 3
52             mov1 = menop3;
53         elseif movltyp == 4
54             mov1 = menop4;
55         elseif movltyp == 5
56             mov1 = menop5;
57         end
58     end
59
60
61

```

```

62     qstring = ['Please load the 10 ' mov1 ' files from the same individual'];
63     button = questdlg(qstring, 'Load movement 1', 'Ok', 'Ok');
64     switch button
65     case 'Ok'
66         % Choose directory for movement 1
67         dir_name = uigetdir('D:\My Documents\BioLab\Tom');
68         cd(dir_name); % Go to chosen directory
69
70         uiopen('LOAD'); % Open 1st file of movement 1
71         movlmat1 = enmat(:);
72
73         uiopen('LOAD'); % Open 2nd file of movement 1
74         movlmat2 = enmat(:);
75
76         uiopen('LOAD'); % Open 3rd file of movement 1
77         movlmat3 = enmat(:);
78
79         uiopen('LOAD'); % Open 4th file of movement 1
80         movlmat4 = enmat(:);
81
82         uiopen('LOAD'); % Open 5th file of movement 1
83         %enmat(isnan(enmat)) = 0;
84         movlmat5 = enmat(:);
85
86         uiopen('LOAD'); % Open 6th file of movement 1
87         %enmat(isnan(enmat)) = 0;
88         movlmat6 = enmat(:);
89
90         uiopen('LOAD'); % Open 7th file of movement 1
91         %enmat(isnan(enmat)) = 0;
92         movlmat7 = enmat(:);
93
94         uiopen('LOAD'); % Open 8th file of movement 1
95         %enmat(isnan(enmat)) = 0;
96         movlmat8 = enmat(:);
97
98         uiopen('LOAD'); % Open 9th file of movement 1
99         movlmat9 = enmat(:);
100
101         uiopen('LOAD'); % Open 9th file of movement 10
102         movlmat0 = enmat(:);
103
104     end
105
106 end
107
108 if m==2 % Generate name string for figures
109     mov2typ = menu(['Movement 2:' ...
110         menuquestrg],menop1,menop2,menop3,menop4,menop5);
111
112     if mov2typ == 1
113         mov2 = menop1;
114
115     elseif mov2typ == 2
116         mov2 = menop2;
117
118     elseif mov2typ == 3
119         mov2 = menop3;
120
121     elseif mov2typ == 4
122         mov2 = menop4;
123
124     elseif mov2typ == 5
125         mov2 = menop5;
126     end
127
128     qstring = ['Please load the 10 ' mov2 ' files from the same individual'];
129     button = questdlg(qstring, 'Load movement 2', 'Ok', 'Ok');
130     switch button
131     case 'Ok'

```

```

131         % Choose directory for movement 2
132         dir_name = uigetdir('D:\My Documents\BioLab\Tom');
133         cd(dir_name);           % Go to choses directory
134
135         uiopen('LOAD');        % Open 1st file of movement 2
136
137         mov2mat1 = enmat(:);
138
139         uiopen('LOAD');        % Open 2nd file of movement 2
140         mov2mat2 = enmat(:);
141
142         uiopen('LOAD');        % Open 3rd file of movement 2
143         mov2mat3 = enmat(:);
144
145         uiopen('LOAD');        % Open 4th file of movement 2
146         mov2mat4 = enmat(:);
147
148         uiopen('LOAD');        % Open 5th file of movement 2
149         mov2mat5 = enmat(:);
150
151         uiopen('LOAD');        % Open 6th file of movement 2
152         mov2mat6 = enmat(:);
153
154         uiopen('LOAD');        % Open 7th file of movement 2
155         mov2mat7 = enmat(:);
156
157         uiopen('LOAD');        % Open 8th file of movement 2
158         mov2mat8 = enmat(:);
159
160         uiopen('LOAD');        % Open 9th file of movement 2
161         mov2mat9 = enmat(:);
162
163         uiopen('LOAD');        % Open 10th file of movement 2
164         mov2mat0 = enmat(:);
165
166         end
167
168     end
169
170     if m==3           % Generate name string for figures
171         mov3typ = menu(['Movement 3:' ...
172             menuquestrg],menop1,menop2,menop3,menop4,menop5);
173
174         if mov3typ == 1
175             mov3 = menop1;
176
177         elseif mov3typ == 2
178             mov3 = menop2;
179
180         elseif mov3typ == 3
181             mov3 = menop3;
182
183         elseif mov3typ == 4
184             mov3 = menop4;
185
186         elseif mov3typ == 5
187             mov3 = menop5;
188         end
189
190     qstring = ['Please load the 10 ' mov3 ' files from the same individual'];
191     button = questdlg(qstring, 'Load movement 3', 'Ok', 'Ok');
192     switch button
193     case 'Ok'
194         % Choose directory for movement 3
195         dir_name = uigetdir('D:\My Documents\BioLab\Tom');
196         cd(dir_name);           % Go to choses directory
197
198         uiopen('LOAD');        % Open 1st file of movement 3
199         mov3mat1 = enmat(:);

```

```

200         uiopen('LOAD');           % Open 2nd file of movement 3
201         mov3mat2 = enmat(:);
202
203         uiopen('LOAD');           % Open 3rd file of movement 3
204         mov3mat3 = enmat(:);
205
206         uiopen('LOAD');           % Open 4th file of movement 3
207         mov3mat4 = enmat(:);
208
209         uiopen('LOAD');           % Open 5th file of movement 3
210         mov3mat5 = enmat(:);
211
212         uiopen('LOAD');           % Open 6th file of movement 3
213         mov3mat6 = enmat(:);
214
215         uiopen('LOAD');           % Open 7th file of movement 3
216         mov3mat7 = enmat(:);
217
218         uiopen('LOAD');           % Open 8th file of movement 3
219         mov3mat8 = enmat(:);
220
221         uiopen('LOAD');           % Open 9th file of movement 3
222         mov3mat9 = enmat(:);
223
224         uiopen('LOAD');           % Open 10th file of movement 3
225         mov3mat0 = enmat(:);
226
227     end
228
229 end
230
231 if m==4                                     % Generate name string for figures
232     mov4typ = menu(['Movement 4:' ...
233                   menuquestrg],menop1,menop2,menop3,menop4,menop5);
234
235     if mov4typ == 1
236         mov4 = menop1;
237
238     elseif mov4typ == 2
239         mov4 = menop2;
240
241     elseif mov4typ == 3
242         mov4 = menop3;
243
244     elseif mov4typ == 4
245         mov4 = menop4;
246
247     elseif mov4typ == 5
248         mov4 = menop5;
249     end
250
251     qstring = ['Please load the 10 ' mov4 ' files from the same individual'];
252     button = questdlg(qstring, 'Load movement 4', 'Ok', 'Ok');
253     switch button
254     case 'Ok'
255         % Choose directory for movement 4
256         dir_name = uigetdir('D:\My Documents\BioLab\Tom');
257         cd(dir_name);           % Go to chosen directory
258
259         uiopen('LOAD');           % Open 1st file of movement 4
260         %enmat(isnan(enmat)) = 0;
261         mov4mat1 = enmat(:);
262
263         uiopen('LOAD');           % Open 2nd file of movement 4
264         %enmat(isnan(enmat)) = 0;
265         mov4mat2 = enmat(:);
266
267         uiopen('LOAD');           % Open 3rd file of movement 4
268         %enmat(isnan(enmat)) = 0;
269         mov4mat3 = enmat(:);

```

```

269
270         uiopen('LOAD');           % Open 4th file of movement 4
271         %enmat(isnan(enmat)) = 0;
272         mov4mat4 = enmat(:);
273
274         uiopen('LOAD');           % Open 5th file of movement 4
275         %enmat(isnan(enmat)) = 0;
276         mov4mat5 = enmat(:);
277
278         uiopen('LOAD');           % Open 6th file of movement 4
279         %enmat(isnan(enmat)) = 0;
280         mov4mat6 = enmat(:);
281
282         uiopen('LOAD');           % Open 7th file of movement 4
283         %enmat(isnan(enmat)) = 0;
284         mov4mat7 = enmat(:);
285
286         uiopen('LOAD');           % Open 8th file of movement 4
287         %enmat(isnan(enmat)) = 0;
288         mov4mat8 = enmat(:);
289
290         uiopen('LOAD');           % Open 9th file of movement 4
291         mov4mat9 = enmat(:);
292
293         uiopen('LOAD');           % Open 10th file of movement 4
294         mov4mat0 = enmat(:);
295
296     end
297
298 end
299
300 if m==5                                     % Generate name string for figures
301     mov5typ = menu(['Movement 5:' ...
302                   menuquestrg],menop1,menop2,menop3,menop4,menop5);
303
304     if mov5typ == 1
305         mov5 = menop1;
306
307     elseif mov5typ == 2
308         mov5 = menop2;
309
310     elseif mov5typ == 3
311         mov5 = menop3;
312
313     elseif mov5typ == 4
314         mov5 = menop4;
315
316     elseif mov5typ == 5
317         mov5 = menop5;
318     end
319
320 qstring = ['Please load the 10 ' mov5 ' files from the same individual'];
321 button = questdlg(qstring, 'Load movement 5', 'Ok', 'Ok');
322 switch button
323     case 'Ok'
324         % Choose directory for movement 5
325         dir_name = uigetdir('D:\My Documents\BioLab\Tom');
326         cd(dir_name);           % Go to chosen directory
327
328         uiopen('LOAD');           % Open 1st file of movement 5
329         %enmat(isnan(enmat)) = 0;
330         mov5mat1 = enmat(:);
331
332         uiopen('LOAD');           % Open 2nd file of movement 5
333         %enmat(isnan(enmat)) = 0;
334         mov5mat2 = enmat(:);
335
336         uiopen('LOAD');           % Open 3rd file of movement 5
337         %enmat(isnan(enmat)) = 0;
338         mov5mat3 = enmat(:);

```

```

338
339         uiopen('LOAD');           % Open 4th file of movement 5
340         %enmat(isnan(enmat)) = 0;
341         mov5mat4 = enmat(:);
342
343         uiopen('LOAD');           % Open 5th file of movement 5
344         %enmat(isnan(enmat)) = 0;
345         mov5mat5 = enmat(:);
346
347         uiopen('LOAD');           % Open 6th file of movement 5
348         %enmat(isnan(enmat)) = 0;
349         mov5mat6 = enmat(:);
350
351         uiopen('LOAD');           % Open 7th file of movement 5
352         %enmat(isnan(enmat)) = 0;
353         mov5mat7 = enmat(:);
354
355         uiopen('LOAD');           % Open 8th file of movement 5
356         %enmat(isnan(enmat)) = 0;
357         mov5mat8 = enmat(:);
358
359         uiopen('LOAD');           % Open 9th file of movement 5
360         mov5mat9 = enmat(:);
361
362         uiopen('LOAD');           % Open 10th file of movement 5
363         mov5mat0 = enmat(:);
364
365     end
366
367 end
368
369 end
370
371 clear enmat mov1typ mov2typ mov3typ mov4typ mov5typ
372 clear menop1 menop2 menop3 menop4 menop5 m menuquestrg
373
374 %% Concatenate energy vector
375 % Create single vector by concatenating all movement vectors
376 % This will constitute column 1 (Variable 1) in the final anovan matrix
377
378 energy = [mov1mat1;mov1mat2;mov1mat3;mov1mat4;mov1mat5           % Movement 1
379          mov1mat6;mov1mat7;mov1mat8;mov1mat9;mov1mat0
380          mov2mat1;mov2mat2;mov2mat3;mov2mat4;mov2mat5           % Movement 2
381          mov2mat6;mov2mat7;mov2mat8;mov2mat9;mov2mat0];
382
383 % Remove unnecessary variables
384 clear mov1mat1 mov1mat2 mov1mat3 mov1mat4 mov1mat5
385 clear mov1mat6 mov1mat7 mov1mat8 mov1mat9 mov1mat0
386 clear mov2mat1 mov2mat2 mov2mat3 mov2mat4 mov2mat5
387 clear mov2mat6 mov2mat7 mov2mat8 mov2mat9 mov2mat0
388
389 % For 3 or more moves
390 if nomov ≥ 3
391
392     energy2 = [mov3mat1;mov3mat2;mov3mat3;mov3mat4;mov3mat5       % Movement 3
393              mov3mat6;mov3mat7;mov3mat8;mov3mat9;mov3mat0];
394
395     % Remove unnecessary variables
396     clear mov3mat1 mov3mat2 mov3mat3 mov3mat4 mov3mat5
397     clear mov3mat6 mov3mat7 mov3mat8 mov3mat9 mov3mat0
398
399     energy = [energy; energy2]; % Add movement 3
400     clear energy2
401
402 end
403
404 % For 4 or more moves
405 if nomov ≥ 4
406
407     energy2 = [mov4mat1;mov4mat2;mov4mat3;mov4mat4;mov4mat5       % Movement 4

```

```

408         mov4mat6;mov4mat7;mov4mat8;mov4mat9;mov4mat0];
409
410     % Remove unnecessary variables
411     clear mov4mat1 mov4mat2 mov4mat3 mov4mat4 mov4mat5
412     clear mov4mat6 mov4mat7 mov4mat8 mov4mat9 mov4mat0
413
414     energy = [energy; energy2]; % Add movement 4
415     clear energy2
416
417     end
418
419     % For 5 moves
420     if nomov == 5
421
422         energy2 = [mov5mat1;mov5mat2;mov5mat3;mov5mat4;mov5mat5 % Movement 5
423                 mov5mat6;mov5mat7;mov5mat8;mov5mat9;mov5mat0];
424
425         % Remove unnecessary variables
426         clear mov5mat1 mov5mat2 mov5mat3
427         clear mov5mat4 mov5mat5 mov5mat6
428         clear mov5mat7 mov5mat8 mov5mat9
429
430         energy = [energy; energy2]; % Add movement 5
431         clear energy2
432
433     end
434
435     energy(isnan(energy)) = 0; % Remove NaNs
436
437     %% Create Scale vector
438     % References a scale value (decomposition bin) for each energy value
439     % Scales run from 1 to 16
440     % This will constitute column 2 (Variable 2) in the final anovan matrix
441
442     % Create matrix of (1 to 16) scales by 103 channels repeated by 10*nomov
443     scale = repmat(1:16,103,10*nomov);
444
445     scale = scale(:); % Convert to column vector
446
447
448     %% Create Channel vector
449     % References a channel to each energy value
450     % Channels run from 1 to 103
451     % This will constitute column 3 (Variable 3) in the final anovan matrix
452
453     % Create vector of (1 to 103) channels repeated by 16 scales * 10*nomov
454     channel = repmat(1:103,1,16*10*nomov);
455
456     channel = channel'; % Transpose into column vector
457
458
459
460     %% Create Movement vector
461     % References a movement to each energy value
462     % This is dependent upon the number of moves (nomov)
463     % This will constitute column 4 (Variable 4) in the final anovan matrix
464
465     % Create vector of (1 to nomov) moves repeated by 103 chan. * 16 scales * 10
466     movement = repmat(1:nomov,10*103*16,1);
467
468     movement = movement(:); % Convert to column vector
469
470     %% Execute 3-way ANOVA analysis on data
471     % Tests for variance across all factors equally
472     % With interactions between movement*scale and movement*channel
473     % Type III sum of squares:
474     % A term = R(B, AB) R(A, B, AB)
475     % B term = R(A, AB) R(A, B, AB)
476     % AB term = R(A, B) R(A, B, AB)
477

```

```

478 varnames = {'Scale';'Channel';'Movement'};           % Assign variable names
479 modtyp = [1 0 0;0 1 0;0 0 1;1 1 1];                 % Set interactions [A;B;C;A*B*C]
480
481 qstring = ['Carry out 3-way ANOVA on ' mov1 ' and ' mov2 '?'];
482 button = questdlg(qstring, 'ANOVA', 'Yes', 'No', 'No');
483 switch button
484     case 'Yes'
485         % Parallel processing toolbox
486         % matlabpool open 4                           % Open 4 cores
487         % ms.UseParallel = 'always'                   % Use parallel processing
488
489         clear qstring questrg                          % Clear unnec. variables
490         energy = single(energy);                       % Convert to single precision
491         [p,table,stats,terms] ...
492         = anovan(energy,{scale channel movement},modtyp,3,varnames);
493
494         % matlabpool close                             % Close cores
495
496         name1 = genvarname(mov1);                      % Create string variable name
497         name1 = name1([1 6:7]);                        % Shorten name1
498         name2 = genvarname(mov2);                      % Create string variable name
499         name2 = name2([1 6:7]);                        % Shorten name2
500         name = [name1 '_X_' name2 '_ANOVA3'];
501
502         if nomov ≥ 3
503             name3 = genvarname(mov3);                  % Create string variable name
504             name3 = name3([1 6:7]);                    % Shorten name3
505             name = [name '_X_' name3 '_ANOVA3'];
506         end
507
508         if nomov ≥ 4
509             name4 = genvarname(mov4);                  % Create string variable name
510             name4 = name4([1 6:7]);                    % Shorten name4
511             name = [name '_X_' name4 '_ANOVA3'];
512         end
513
514         if nomov == 5
515             name5 = genvarname(mov5);                  % Create string variable name
516             name5 = name5([1 6:7]);                    % Shorten name5
517             name = [name '_X_' name5 '_ANOVA3'];
518         end
519
520         questr = ['Save details as: ' name '_ANOVA3?'];
521         namebutton = questdlg(questr, 'Name?', 'yes', 'no', 'yes');
522         switch namebutton
523             case 'yes'
524                 % Keep automatic string name
525             case 'no'
526                 name = input('Save figure and coefficients as? ','s');
527                 % Enter new name
528         end
529
530         save(plotname, 'enmat');                       % Save energy matrix (current ...
531         dir)
532     case 'No'
533         disp('Thanks for using this program')
534 end

```

Bibliography

- [1] Addison, P., J. Walker, and R. Guido (2009). Time-frequency analysis of biosignals. *Engineering in Medicine and Biology Magazine, IEEE* 28(5), 14–29.
- [2] Blok, J., J. Van Dijk, G. Drost, M. Zwarts, and D. Stegeman (2002). A high-density multichannel surface electromyography system for the characterization of single motor units. *Review of scientific instruments* 73, 1887.
- [3] Bofill, P. and M. Zibulevsky (2001). Underdetermined blind source separation using sparse representations. *Signal processing* 81(11), 2353–2362.
- [4] Bruce, A., D. Donoho, and H.-Y. Gao (1996, oct). Wavelet analysis [for signal processing]. *Spectrum, IEEE* 33(10), 26–35.
- [5] Carlson, N. (2001). *Physiology of behavior*. Allyn & Bacon.
- [6] Croft, A., R. Davison, and M. Hargreaves (1996). *Engineering mathematics*. Addison-Wesley.
- [7] Datta, S., I. Lyon, B. Mackintosh, H. McLannahan, K. Murphy, P. Naish, D. Nettle, I. Romero, F. Toates, and T. Watson (2007a). *From Cells To Consciousness*. Milton Keynes, The Open University.
- [8] Datta, S., I. Lyon, B. Mackintosh, H. McLannahan, K. Murphy, P. Naish, D. Nettle, I. Romero, F. Toates, and T. Watson (2007b). *From Neurons To Behaviour*. Milton Keynes, The Open University.
- [9] De Luca, C. (1997). The use of surface electromyography in biomechanics. *Journal of Applied Biomechanics* 13, 135–163.
- [10] Drost, G., J. Blok, D. Stegeman, J. Van Dijk, B. van Engelen, and M. Zwarts (2001). Propagation disturbance of motor unit action potentials during transient paresis in generalized myotonia. *Brain* 124(2), 352.
- [11] Drost, G., D. Stegeman, M. Schillings, H. Horemans, H. Janssen, M. Massa, F. Nollet, and M. Zwarts (2004). Motor unit characteristics in healthy subjects and those with post-poliomyelitis syndrome: A high-density surface emg study. *Muscle & nerve* 30(3), 269–276.
- [12] Ekštein, K. and T. Pavelka (2004). Entropy and entropy-based features in signal processing. In *Proceedings of PhD Workshop Systems & Control*.
- [13] Farina, D. and D. Falla (2008). Estimation of muscle fiber conduction velocity from two-dimensional surface emg recordings in dynamic tasks. *Biomedical Signal Processing and Control* 3(2), 138–144.
- [14] Farina, D., A. Holobar, R. Merletti, and R. Enoka (2010). Decoding the neural drive to muscles from the surface electromyogram. *Clinical Neurophysiology* 121(10), 1616–1623.
- [15] Farina, D., F. Negro, M. Gazzoni, and R. Enoka (2008). Detecting the unique representation of motor-unit action potentials in the surface electromyogram. *Journal of neurophysiology* 100(3), 1223.
- [16] FitzGerald, M. (1995). *Neuroanatomy: basic and clinical*. WB Saunders Company.
- [17] Flanders, M. (2002). Choosing a wavelet for single-trial emg. *Journal of neuroscience methods* 116(2), 165–177.

- [18] García, G., R. Okuno, and K. Azakawa (2005). A decomposition algorithm for surface electrode-array electromyogram. *Engineering in Medicine and Biology Magazine, IEEE* 24(4), 63–72.
- [19] Gazzoni, M., D. Farina, and R. Merletti (2004). A new method for the extraction and classification of single motor unit action potentials from surface emg signals. *Journal of neuroscience methods* 136(2), 165–177.
- [20] Graps, A. (1995). An introduction to wavelets. *Computational Science & Engineering, IEEE* 2(2), 50–61.
- [21] Grönlund, C., N. Östlund, K. Roeleveld, and J. Karlsson (2005). Simultaneous estimation of muscle fibre conduction velocity and muscle fibre orientation using 2d multichannel surface electromyogram. *Medical and Biological Engineering and Computing* 43(1), 63–70.
- [22] Guzmán, R., R. Silvestre, and D. Arriagada (2011). Biceps brachii muscle innervation zone location in healthy subjects using high-density surface electromyography. *International Journal of Morphology* 29(2), 347–352.
- [23] Hodson-Tole, E. and J. Wakeling (2009). Motor unit recruitment for dynamic tasks: current understanding and future directions. *Journal of Comparative Physiology B: Biochemical, Systemic, and Environmental Physiology* 179(1), 57–66.
- [24] Holobar, A., D. Farina, M. Gazzoni, R. Merletti, and D. Zazula (2009). Estimating motor unit discharge patterns from high-density surface electromyogram. *Clinical Neurophysiology* 120(3), 551–562.
- [25] Holobar, A., M. Minetto, A. Botter, F. Negro, and D. Farina (2010). Experimental analysis of accuracy in the identification of motor unit spike trains from high-density surface emg. *Neural Systems and Rehabilitation Engineering, IEEE Transactions on* 18(3), 221–229.
- [26] Holobar, A. and D. Zazula (2004). Correlation-based decomposition of surface electromyograms at low contraction forces. *Medical and Biological Engineering and Computing* 42(4), 487–495.
- [27] Holobar, A. and D. Zazula (2007). Multichannel blind source separation using convolution kernel compensation. *Signal Processing, IEEE Transactions on* 55(9), 4487–4496.
- [28] Hu, X., Y. Gao, and W. Liu (2009). Pattern recognition of surface electromyography signal based on wavelet coefficient entropy. *Health* 1(2), 121–126.
- [29] Hu, X., Z. Wang, and X. Ren (2005). Classification of surface emg signal using relative wavelet packet energy. *Computer methods and programs in biomedicine* 79(3), 189–195.
- [30] Huang, H., P. Zhou, G. Li, and T. Kuiken (2008). An analysis of emg electrode configuration for targeted muscle reinnervation based neural machine interface. *Neural Systems and Rehabilitation Engineering, IEEE Transactions on* 16(1), 37–45.
- [31] Huang, H., P. Zhou, G. Li, and T. Kuiken (2009). Spatial filtering improves emg classification accuracy following targeted muscle reinnervation. *Annals of biomedical engineering* 37(9), 1849–1857.
- [32] Keenan, K., D. Farina, R. Merletti, and R. Enoka (2006). Amplitude cancellation reduces the size of motor unit potentials averaged from the surface emg. *Journal of Applied Physiology* 100(6), 1928.
- [33] Kleine, B., J. Blok, R. Oostenveld, P. Praamstra, and D. Stegeman (2000). Magnetic stimulation-induced modulations of motor unit firings extracted from multi-channel surface emg. *Muscle & nerve* 23(7), 1005–1015.

- [34] Kleine, B., D. Stegeman, G. Drost, and M. Zwarts (2008). Interspike interval analysis in a patient with peripheral nerve hyperexcitability and potassium channel antibodies. *Muscle & nerve* 37(2), 269–274.
- [35] Kleine, B., J. van Dijk, B. Lapatki, M. Zwarts, and D. Stegeman (2007). Using two-dimensional spatial information in decomposition of surface emg signals. *Journal of Electromyography and Kinesiology* 17(5), 535–548.
- [36] Kleine, B., J. van Dijk, M. Zwarts, and D. Stegeman (2008). Inter-operator agreement in decomposition of motor unit firings from high-density surface emg. *Journal of Electromyography and Kinesiology* 18(4), 652–661.
- [37] Kolmogorov, A. and S. Fomin (1975). *Introductory real analysis*. Dover Pubns.
- [38] Lapatki, B., J. Van Dijk, I. Jonas, M. Zwarts, and D. Stegeman (2004). A thin, flexible multielectrode grid for high-density surface emg. *Journal of Applied Physiology* 96(1), 327.
- [39] Maathuis, E. M., J. Drenthen, J. P. van Dijk, G. H. Visser, and J. H. Blok (2008). Motor unit tracking with high-density surface emg. *Journal of Electromyography and Kinesiology* 18(6), 920 – 930. 2008 ISEK Congress Keynote Lecture.
- [40] Masuda, T. and T. Sadoyama (1988). Topographical map of innervation zones within single motor units measured with a grid surface electrode. *Biomedical Engineering, IEEE Transactions on* 35(8), 623–628.
- [41] Merletti, R., A. Holobar, and D. Farina (2008). Analysis of motor units with high-density surface electromyography. *Journal of Electromyography and Kinesiology* 18(6), 879–890.
- [42] Micera, S., J. Carpaneto, and S. Raspopovic (2010). Control of hand prostheses using peripheral information. *Biomedical Engineering, IEEE Reviews in* 3, 48 –68.
- [43] Nagata, K., K. Adno, M. Yamada, and K. Magatani (2005). A classification method of hand movements using multi channel electrode. In *Engineering in Medicine and Biology Society, 2005. IEEE-EMBS 2005. 27th Annual International Conference of the*, pp. 2375–2378. IEEE.
- [44] Nagata, K., K. Ando, K. Magatani, and M. Yamada (2007). Development of the hand motion recognition system based on surface emg using suitable measurement channels for pattern recognition. In *Engineering in Medicine and Biology Society, 2007. EMBS 2007. 29th Annual International Conference of the IEEE*, pp. 5214–5217. IEEE.
- [45] Ochkov, V. (2007). *Mathcad 14 for students, engineers and designers*. spb.
- [46] Prutchi, D. (1995). A high-resolution large array (hrla) surface emg system. *Medical engineering & physics* 17(6), 442–454.
- [47] Reucher, H., G. Rau, and J. Silny (1987). Spatial filtering of noninvasive multielectrode emg: Part i-introduction to measuring technique and applications. *Biomedical Engineering, IEEE Transactions on* (2), 98–105.
- [48] Roeleveld, K., J. Blok, D. Stegeman, and A. Van Oosterom (1997). Volume conduction models for surface emg; confrontation with measurements1. *Journal of Electromyography and Kinesiology* 7(4), 221–232.
- [49] Roeleveld, K., A. Sandberg, E. Stålberg, and D. Stegeman (1998). Motor unit size estimation of enlarged motor units with surface electromyography. *Muscle & nerve* 21(7), 878–886.
- [50] Roeleveld, K. and D. Stegeman (2002). What do we learn from motor unit action potentials in surface electromyography? *Muscle & nerve* 25(S11), S92–S97.
- [51] Ryall, R. (1981). Patterns of recurrent excitation and mutual inhibition of cat rensaw cells. *The Journal of Physiology* 316(1), 439.

- [52] Sörnmo, L. and P. Laguna (2006). *Bioelectrical signal processing in cardiac and neurological applications*. Elsevier Academic Press.
- [53] Tenore, F., A. Ramos, A. Fahmy, S. Acharya, R. Etienne-Cummings, and N. Thakor (2007). Towards the control of individual fingers of a prosthetic hand using surface emg signals. In *Engineering in Medicine and Biology Society, 2007. EMBS 2007. 29th Annual International Conference of the IEEE*, pp. 6145–6148. IEEE.
- [54] van Dijk, J., J. Blok, B. Lapatki, I. van Schaik, M. Zwarts, and D. Stegeman (2008). Motor unit number estimation using high-density surface electromyography. *Clinical Neurophysiology* 119(1), 33–42.
- [55] Vander, A., J. Sherman, D. Luciano, M. Kluger, and L. G. d’Alecy (1990). *Human physiology: the mechanisms of body function*. McGraw-Hill New York etc.
- [56] Vidakovic, B. and P. Mueller (1991). Wavelets for kids. *A Tutorial Introduction, Institute of Statistics and Decision Science, Duke University, Durham, NC*.
- [57] Wakeling, J. (2009). Patterns of motor recruitment can be determined using surface emg. *Journal of Electromyography and Kinesiology* 19(2), 199–207.
- [58] Wood, S., J. Jarratt, A. Barker, and B. Brown (2001). Surface electromyography using electrode arrays: a study of motor neuron disease. *Muscle & nerve* 24(2), 223–230.
- [59] Young, H., R. Freedman, and L. Ford (2006). *University physics*, Volume 1. Addison Wesley Longman.
- [60] Zhang, X., Y. Wang, and R. Han (2010, aug.). Wavelet transform theory and its application in emg signal processing. In *Fuzzy Systems and Knowledge Discovery (FSKD), 2010 Seventh International Conference on*, Volume 5, pp. 2234 –2238.
- [61] Zhou, P., M. Lowery, J. Dewald, and T. Kuiken (2005). Towards improved myoelectric prosthesis control: High density surface emg recording after targeted muscle reinnervation. In *Engineering in Medicine and Biology Society, 2005. IEEE-EMBS 2005. 27th Annual International Conference of the*, pp. 4064–4067. IEEE.
- [62] Zwarts, M. and D. Stegeman (2003). Multichannel surface emg: basic aspects and clinical utility. *Muscle & nerve* 28(1), 1–17.